Supporting Information

Design, synthesis, enzymatic and in vivo antihyperglycemic activity evaluation of 1,3,4-Oxadiazole Derivatives Targeting Multiple Pathways in Type 2 Diabetes

Shereen [a], Ayesha Tahir [b], Awais Ahmed [b], Muhammad Saeed Jan [c], Nouman Aslam [b], Sohail Hassan[*a], Umer Rashid[b]**

[a]Department of Pharmaceutical Chemistry, Faculty of Pharmacy and Pharmaceutical Sciences, University of Karachi, Karachi- 75270, Pakistan

[b]Department of Chemistry, COMSATS University Islamabad, Abbottabad Campus, 22060 Abbottabad, Pakistan. E-mail:

[c]Department of Pharmacy, University of Swabi, Anbar, 23430, Khyber Pakhtunkhwa, Pakistan.

Corresponding Authors:

shassan@uok.edu.pk (Sohail Hassan)

umerrashid@cuiatd.edu.pk (Umer Rashid)

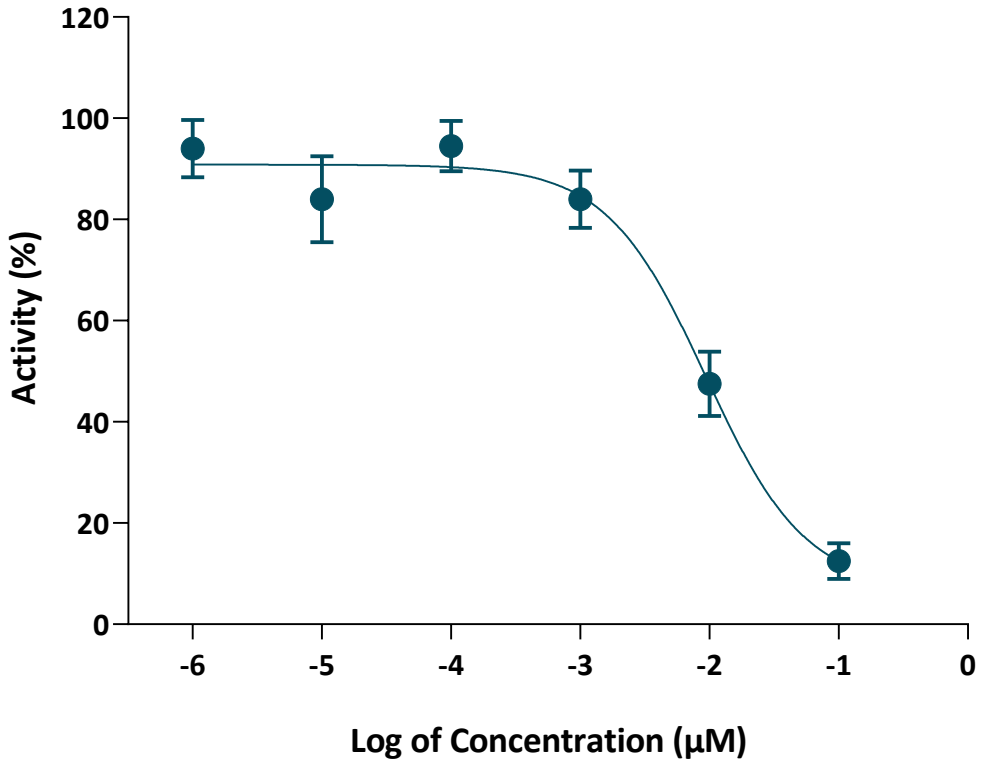

Figure S-1. Dose-response curve of Sitagliptin (standard drug) against DPP-4.

Comparison of binding modes of 18 and 23 in terms of the common motifs against α-amylase

Within the α-amylase active site, compound **23** establishes a more extensive hydrogen-bonding network compared to **18**, though **18** uniquely targets a critical catalytic residue. Compound **18** forms a rare and significant π–anion interaction between its oxadiazole ring and the acid-base catalytic residue Glu233, an interaction not observed for **23**. Conversely, **23** exhibits superior polar interaction potential via its CF_3 group, which forms a hydrogen bond with His101 and halogen bonds with Tyr62 and Asp197, whereas **18**'s CF_3 is limited to a single halogen bond with Tyr62. The THP core of 18 interacts with Asp300 (substrate binding), while **23**'s core engages Gln63 and Tyr62, both of which are part of the established catalytic environment. Finally, the benzohydrazide moiety in **23** provides strong anchoring at the peripheral region of the binding cleft via three hydrogen bonds with Tyr151 and Ile235, in contrast to **18**'s more modest

interactions with Lys200 and Glu240.

Table S-1: Receptor residues for each common motif of compounds **18** and **23** against α-amylase

Common motifs	**Compound 18**	**Compound 23**
CF_3	TYR62 (Halogen-F)	HIS101 (Conventional H-bond) TYR62 (Halogen-F) ASP197 (Halogen-F)
THP core	ASP300 (Conventional H-bond)	GLN63 (Conventional H-bond) TYR62 (Conventional-H)
Oxadiazole ring	GLU233 (π-anion)	-----
Benzohydrazide	LYS200 (Conventional H-bond) GLU240 (Conventional H-bond)	ILE235 (Conventional-H, Conventional-H) TYR151 (Conventional H-bond)

Comparison of binding modes of 18 and 23 in terms of the common motifs against α-glucosidase

In the active site of α-glucosidase, compounds **18** and **23** demonstrate distinct binding strategies despite utilizing common motifs, with **18** primarily anchoring to the catalytic triad while **23** relies more heavily on halogen-mediated stabilization. Compound **18** leverages its tetrahydropyrimidine (THP) core to engage the enzyme's catalytic triad through conventional hydrogen bonds with Asp349 and Glu276, whereas **23** utilizes the same core to interact with Arg439. The trifluoromethyl (CF_3) group in **18** forms a simple hydrogen bond with Arg312, but in **23**, it establishes an extensive network of four halogen–fluorine interactions with Asp408 and Phe157, a strategy known to reinforce binding strength via non-covalent halogen bonding. Furthermore, the oxadiazole ring which is a common bioisostere for amide groups participates in π–π stacking with Phe300 for both compounds, though only **18** forms an additional hydrogen bond with His279, while **23** interacts with Arg312. The benzohydrazide moiety provides further differentiation, with **18** forming hydrogen bonds with Phe310 and Arg312, while **23** anchors more deeply into the substrate-binding pocket via Pro309 and aromatic interactions with Trp242.

Table S-2: Receptor residues for each common motif of compounds **18** and **23** against α-glucosidase

Common motifs	Compound 18	Compound 23
CF_3	ARG312 (Conventional H-bonds) ASP349 (Halogen-F)	ASP408 (Halogen-F, Halogen-F) PHE157 (Halogen-F, Halogen-F, π-π Stacked)
THP core	ASP349 (Conventional-H) GLU276 (Conventional H-bond)	ARG439 (Conventional H-bond)
Oxadiazole ring	HIS279 (Conventional H-bond) PHE300 (π-π Stacked)	ARG312 (Conventional H-bond) PHE300 (π-π T-Shaped)
Benzohydrazide	ARG312 (Conventional H-bonds) PHE310 (Conventional H-bond)	PRO309 (Conventional H-bond)

Comparison of binding modes of 18 and 23 in terms of the common motifs against DPP-4

The comparison in DPP4 centers on subsite specificity, where 18 displays broad subsite interaction while **23** mimics the binding pattern of established drugs like Sitagliptin. The CF_3 group is a dominant contributor for **18**, establishing four interactions across Arg125, Asn710, Glu205, and His740, whereas the provided data shows no specific CF_3 interactions for **23**. Compound **18** also stabilizes itself within the S1 subsite by forming hydrogen bonds between its THP core and the essential catalytic residue Ser630. While both compounds utilize their oxadiazole and benzohydrazide motifs to interact with Phe357 via π–π stacking, **23** establishes a firmer anchor within the S2-extensive subsite through strong hydrogen bonds with Arg358 and Ser209. This strategic occupancy of the S1 and S2-extensive sub-pockets by **23** reinforces its potential as a potent inhibitor by aligning with the molecular rationale of high-affinity DPP4 inhibitors.

Table S-3: Receptor residues for each common motif of compounds **18** and **23** against **DPP-4**

Common motifs	**Compound 18**	**Compound 23**
CF_3	ASN710 (Conventional H-bond) ARG125 (Conventional H-bond) GLU205 (Halogen-F) HIS740 (Halogen-F)	-----
THP core	SER630 (Conventional H-bonds)	-----
Oxadiazole ring	-----	PHE357 (π-π Stacked)
Benzohydrazide	VAL207 (Conventional H-bond) GLU206 (Conventional H-bond) PHE357 (π-π Stacked)	ARG358(Conventional H-bond) SER209 (Conventional H-bond) PHE357 (π-π Stacked)

Comparison of binding modes of 18 and 23 in terms of the common motifs against PTP-1B

Although analogs **18** and **23** share common motifs, they occupy entirely different regions of the PTP1B binding site, resulting in distinct inhibitory mechanisms. Compound **18** acts as a multisite binder, demonstrating a broad binding profile that spans from the catalytic (A site) to the adjacent noncatalytic regions (B–D sites). Its pose is characterized by its hydrazide moiety establishing bonds at the peripheral B-D region (Asp29, Phe30) while its oxadiazole ring and aromatic core interact with Arg254, Gly259, and Met258 near the B-site. In contrast, **23** is strictly localized within the catalytic domain and its signature loops; it anchors specifically to the WPD loop via Gly183 and the phosphate-binding loop via Cys215 and Arg221. While **18** stabilizes the protein through extensive multisite interactions including Gln262 and Lys36, **23** focuses on the catalytic residue Asp48 and a peripheral pocket near Ala217, behaving as a more traditional active-site inhibitor.

Table S-4: Receptor residues for each common motif of compounds **18** and **23** against **PTP-1B**

Common motifs	**Compound 18**	**Compound 23**
CF_3	ASP48 (Halogen-F interactions)	GLY183 (Halogen-F, Halogen-F) GLN266 (Conventional-H, Halogen-F)
THP core	GLN262 (Conventional H-bond)	GLY183 (Conventional-H bond)
Oxadiazole ring	GLY259 (Conventional H-bond) ARG254 (Conventional H-bond) MET258 (π-sigma)	-----
Benzohydrazide	MET258 (π-sulfur) LYS36 (Conventional H-bond) ASP29 (Conventional H-bond) PHE30 (Conventional H-bond)	ASP48 (Conventional H-bond)

Table S-5: Binding energy values and interacting residues along with their types and bond distances for synthesized compounds **18** and **23** against the biological targets.

Biological Target	Compound18			Compound 23		
	S value	**Interacting residues and types**	**Bond Distance**	**S value**	**Interacting residues and types**	**Bond Distance**
α-Amylase	-6.405	LYS200 (Conventional H-bond) ASP300 (Conventional H-bond) GLU240 (Conventional H-bond) TYR62 (Halogen-F) GLU233 (π-anion)	2.06 2.44 3.06 3.54 4.19	-7.877	ILE235 (Conventional-H, Conventional-H) HIS101 (Conventional H-bond) GLN63 (Conventional H-bond) TYR62 (Conventional-H, Halogen-F) TYR151 (Conventional H-bond) ASP197 (Halogen-F) TRP59 (π-π T-Shaped)	2.30, 2.62 2.34 2.41 2.51, 3.47 2.87 3.28 5.03
α-Glucosidase	-6.158	ARG312 (Conventional H-bonds) ASP349 (Conventional-H, Halogen-F) PHE310 (Conventional H-bond) GLU276 (Conventional H-bond) HIS279 (Conventional H-bond) PHE300 (π-π Stacked)	2.03, 2.86 2.54, 3.42 2.09 2.28 2.59 4.37	-8.071	ARG312 (Conventional H-bond) ARG439 (Conventional H-bond) PRO309 (Conventional H-bond) ASP408 (Halogen-F, Halogen-F) PHE157 (Halogen-F, Halogen-F, π-π Stacked) HIS239 (π-π T-Shaped) PHE300 (π-π T-Shaped) TRP242 (π-sigma, π-π T-Shaped)	2.15 2.25 2.74 2.71, 2.89 2.81, 3.30, 5.12 4.96 5.15 2.89, 5.33
DPP4	-6.074	SER630 (Conventional H-bonds) VAL207 (Conventional H-bond) GLU206 (Conventional H-bond) ASN710 (Conventional H-bond) ARG125 (Conventional H-bond) GLU205 (Halogen-F) HIS740 (Halogen-F) PHE357 (π-π Stacked)	2.16, 2.72 2.03 2.82 2.91 6.62 2.91 2.93 4.23	-8.725	ARG358(Conventional H-bond) SER209 (Conventional H-bond) PHE357 (π-π Stacked, π-π Stacked) TYR666 (π-π T-Shaped) TYR662 (π-π Stacked)	2.49 2.97 4.72, 5.18 5.18 5.36
PTP1B	-5.155	PHE30 (Conventional H-bonds) LYS36 (Conventional H-bond) GLN262 (Conventional H-bond) GLY259 (Conventional H-bond) ASP29 (Conventional H-bond) ARG254 (Conventional H-bond) ASP48 (Halogen-F interactions) MET258 (π-sigma, π-sulfur)	2.22, 3.05 2.15 2.22 2.49 2.69 3.00 3.08, 3.28, 3.50 2.56, 4.17	-6.622	ASP48 (Conventional H-bond) GLN266 (Conventional-H, Halogen-F) GLY183 (Conventional-H, Halogen-F, Halogen-F) ALA217 (Conventional H-bond) SER216 (Conventional H-bond) ARG221 (π-cation) CYS215 (π-sulfur)	1.89 2.27, 3.48 2.28, 2.66, 3.37 2.39 2.70 4.23 5.71

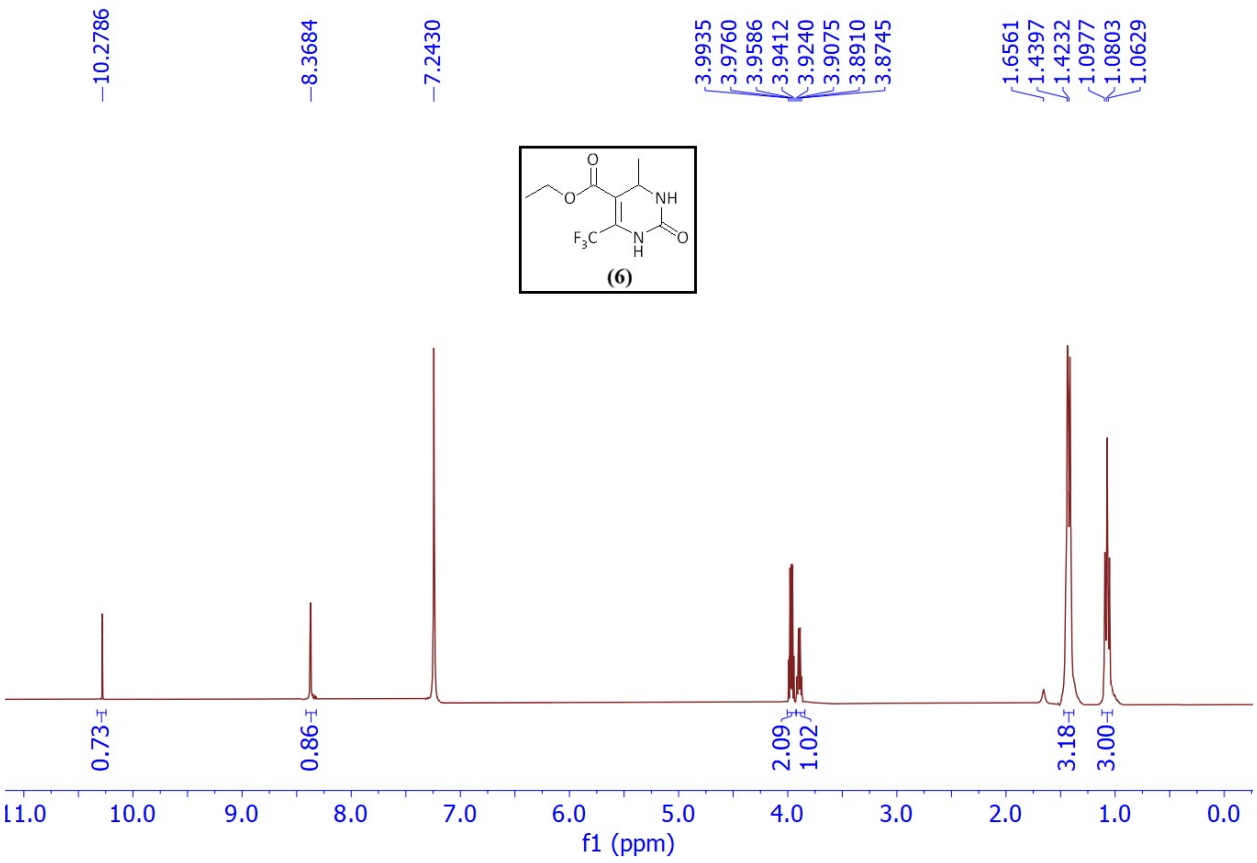

Figure S-2. ^{1}H NMR (400 MHz, $CDCl_3$) spectrum of Intermediate **6.**

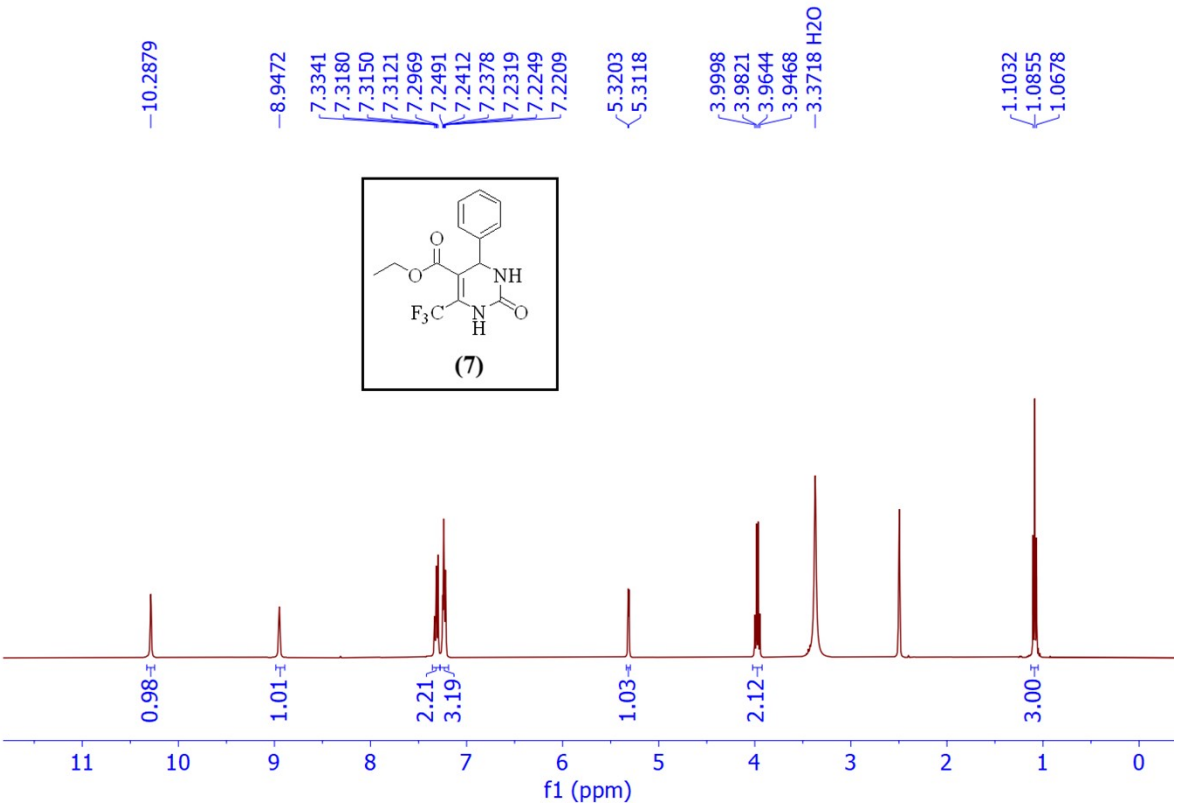

Figure S-3. ^{1}H NMR (400 MHz, DMSO-d_6) spectrum of Intermediate **7.**

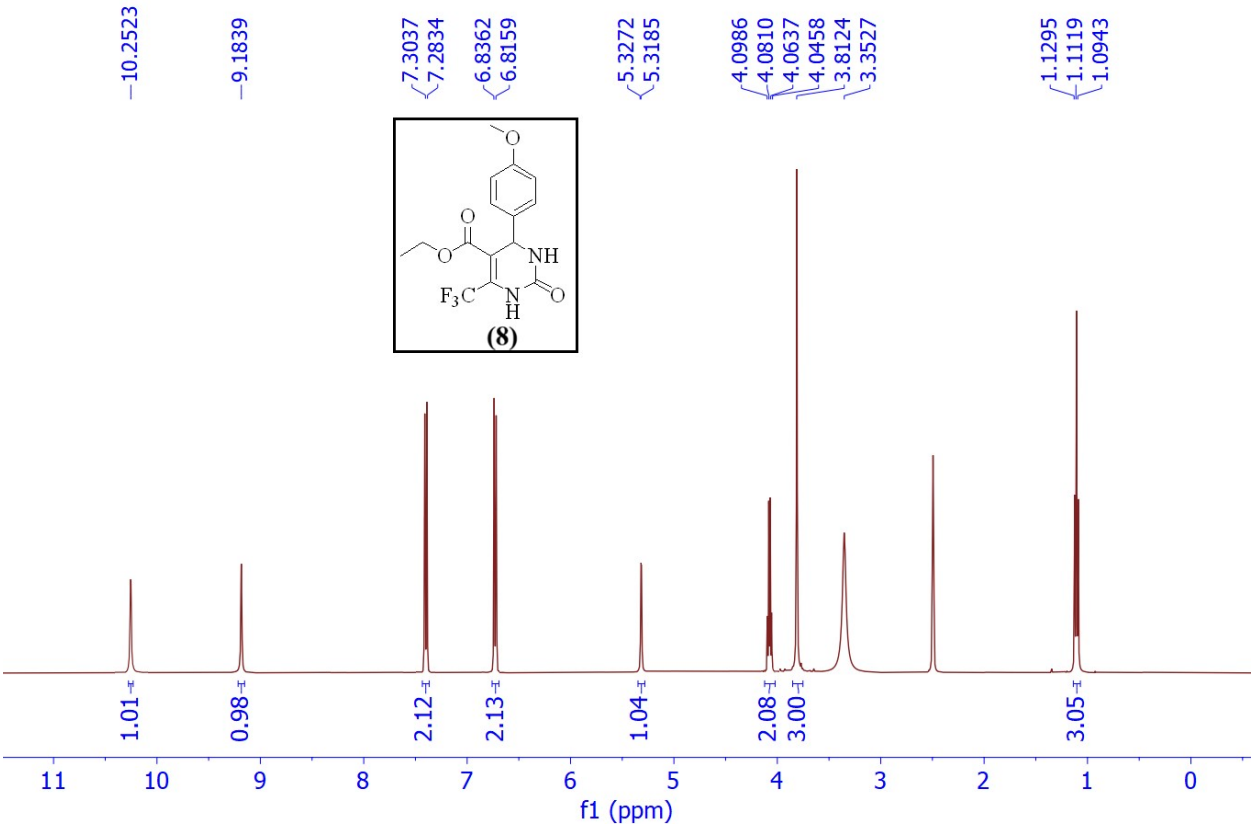

Figure S-4. ^{1}H NMR (400 MHz, DMSO-d_6) spectrum of Intermediate **8.**

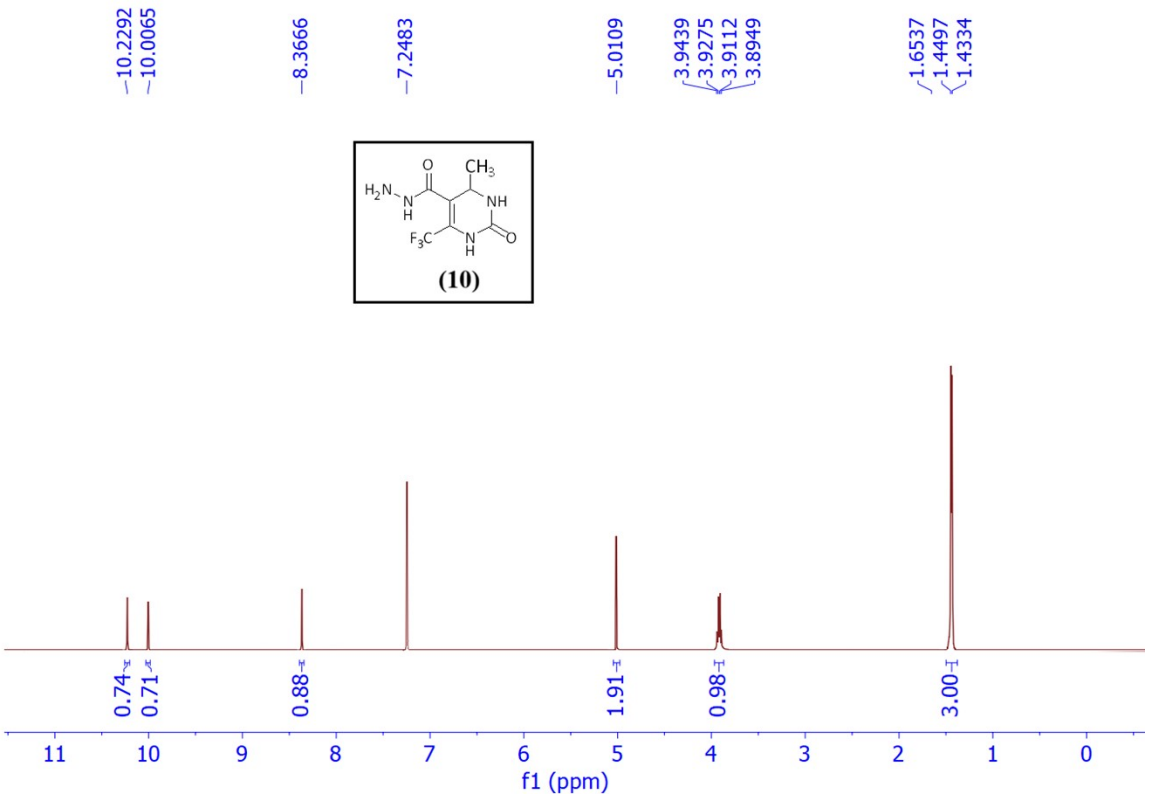

Figure S-5. ^{1}H NMR (400 MHz, DMSO-d_6) spectrum of Intermediate **10.**

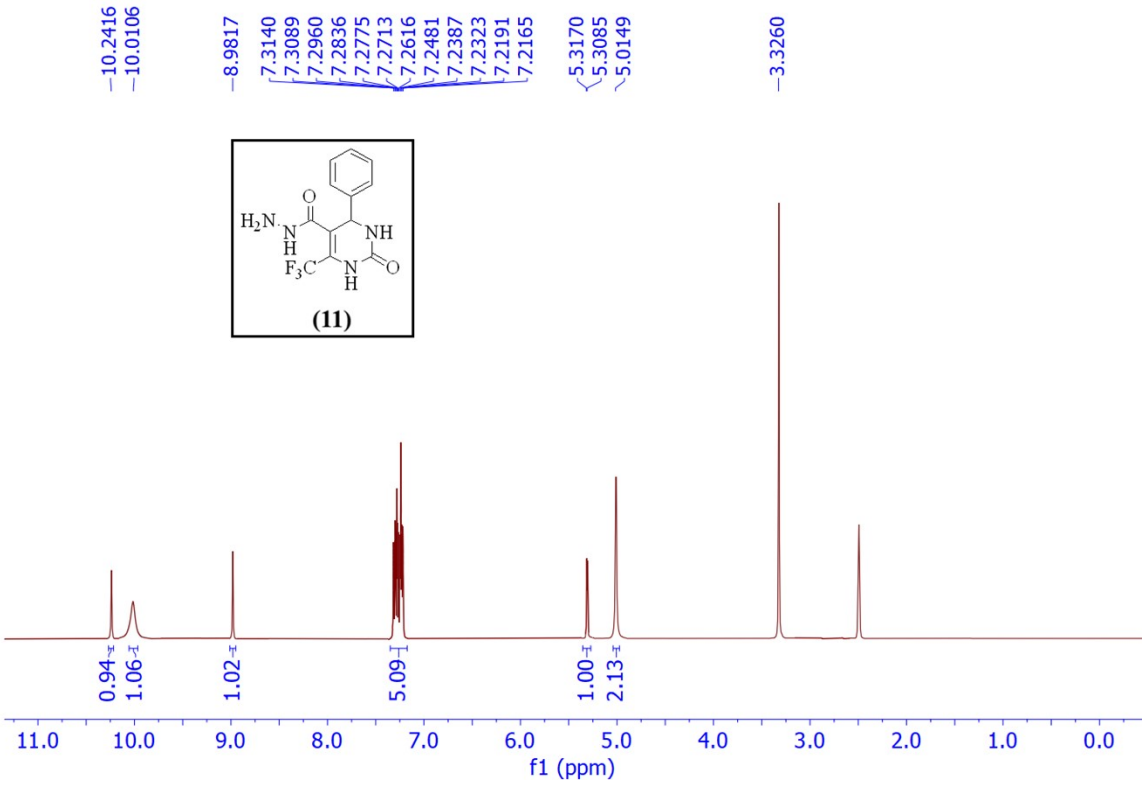

Figure S-6. ^{1}H NMR (400 MHz, DMSO-d_6) spectrum of Intermediate **11.**

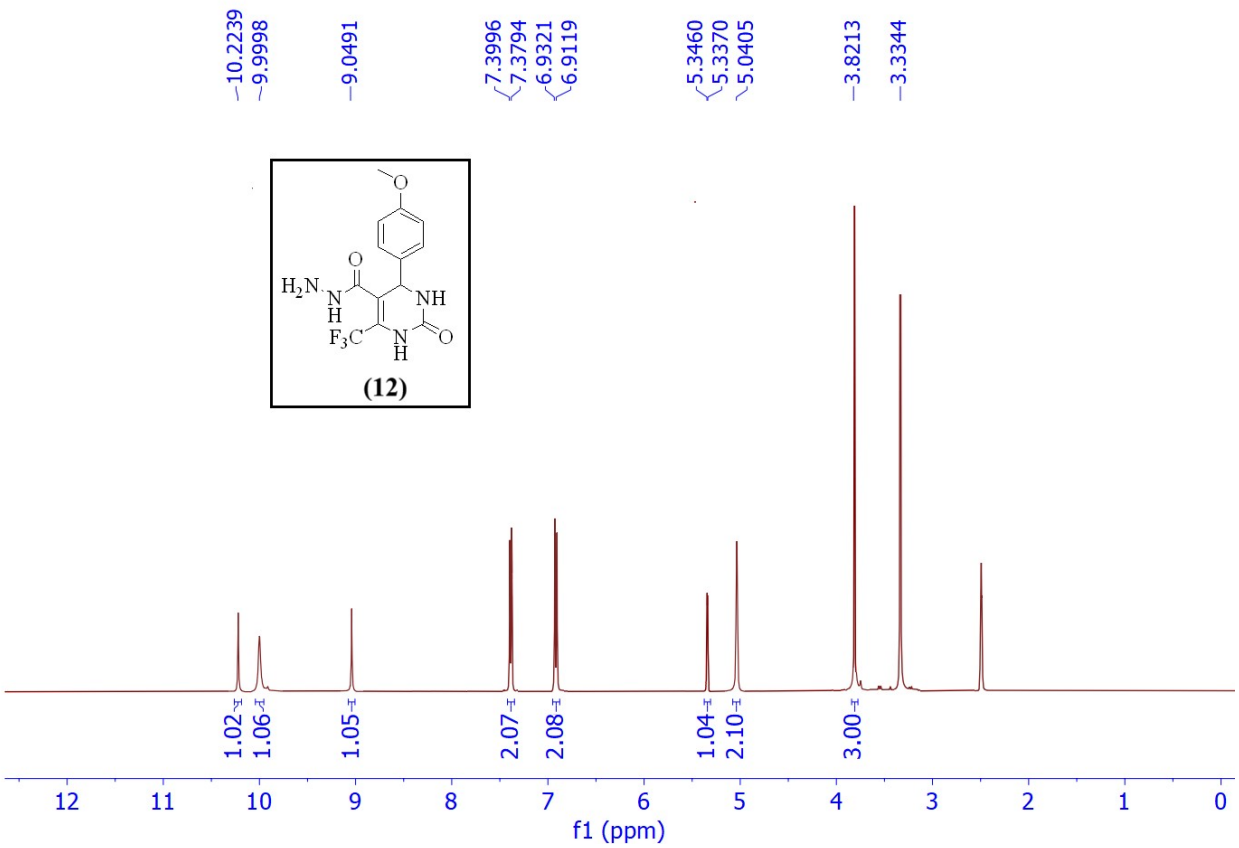

Figure S-7. ^{1}H NMR (400 MHz, DMSO-d_6) spectrum of Intermediate **12.**

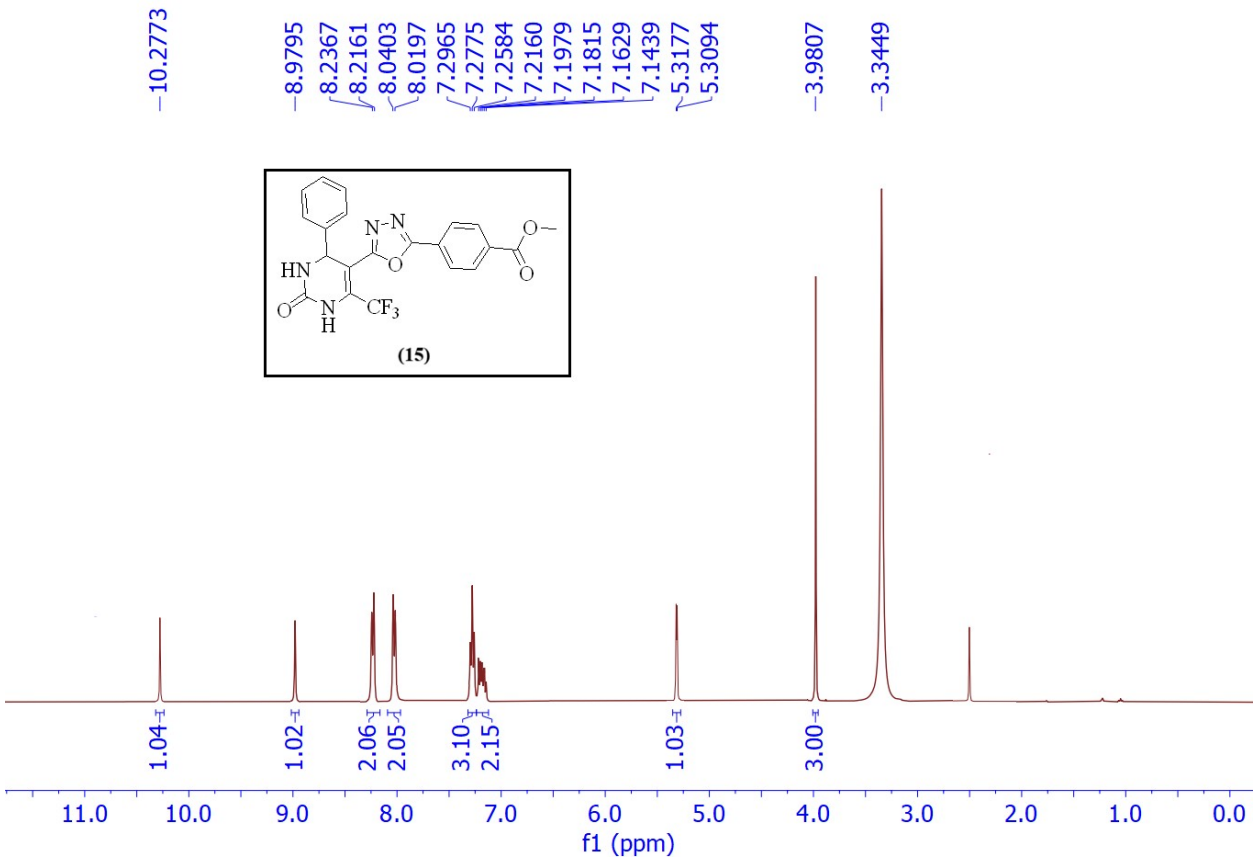

Figure S-8. ^{1}H NMR (400 MHz, DMSO-d_6) spectrum of Intermediate **15.**

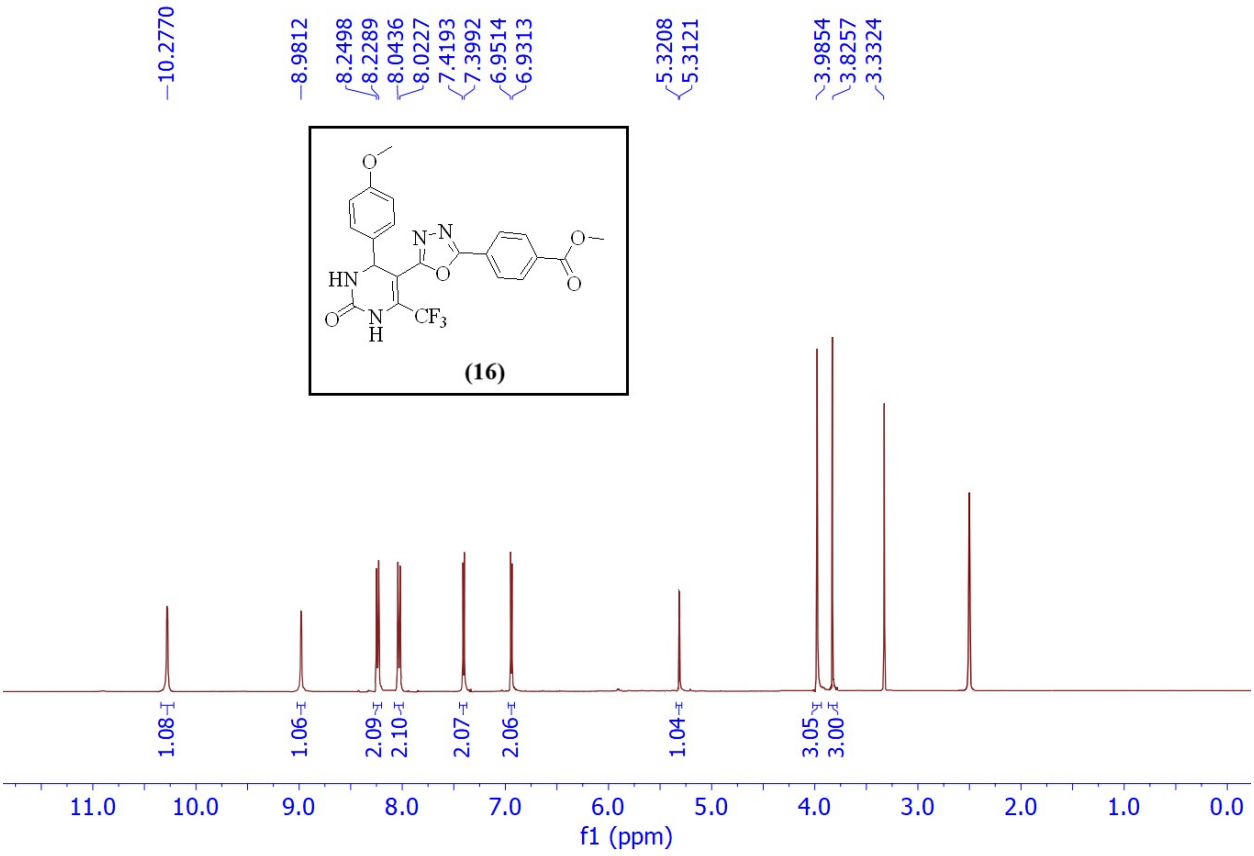

Figure S-9. ^{1}H NMR (400 MHz, DMSO-d_6) spectrum of Intermediate **16.**

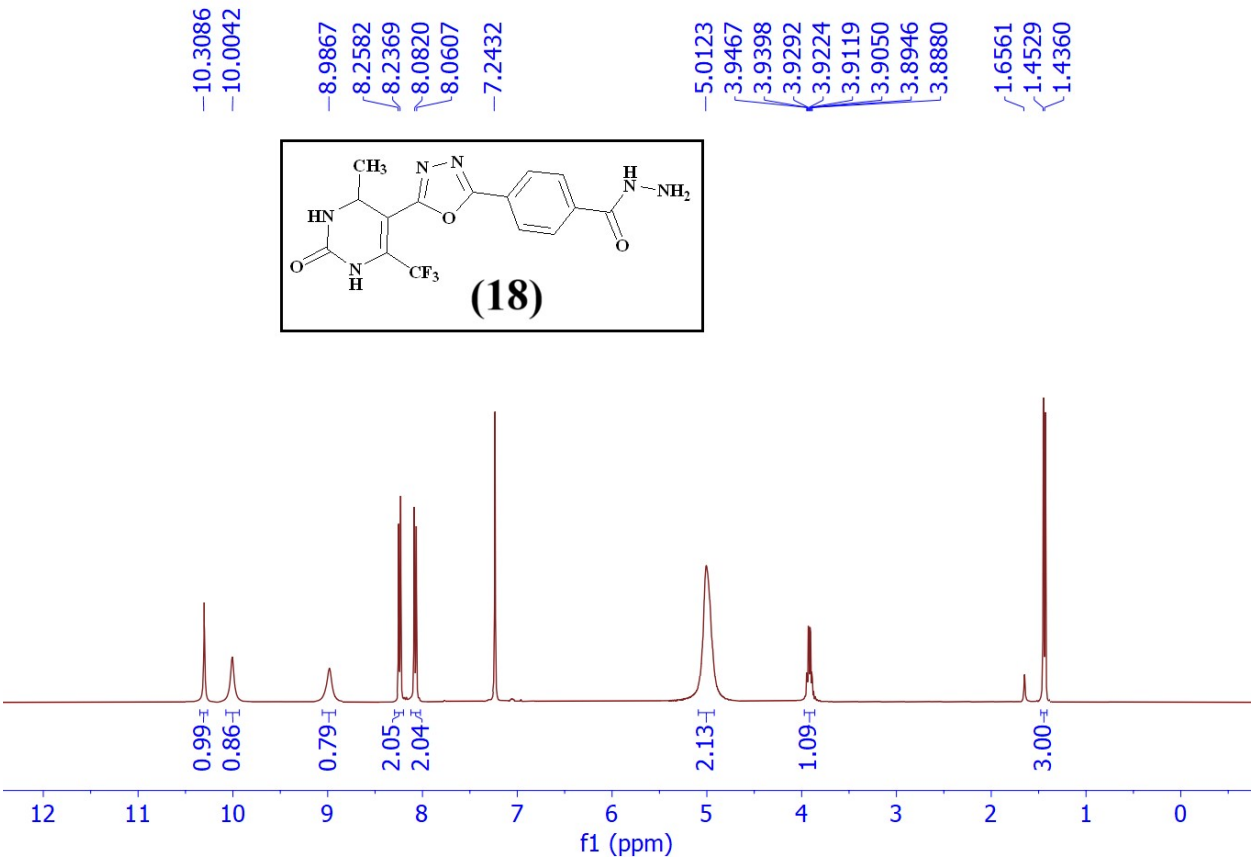

Figure S-10. ^{1}H NMR (400 MHz, $CDCl_3$) spectrum of compound **18.**

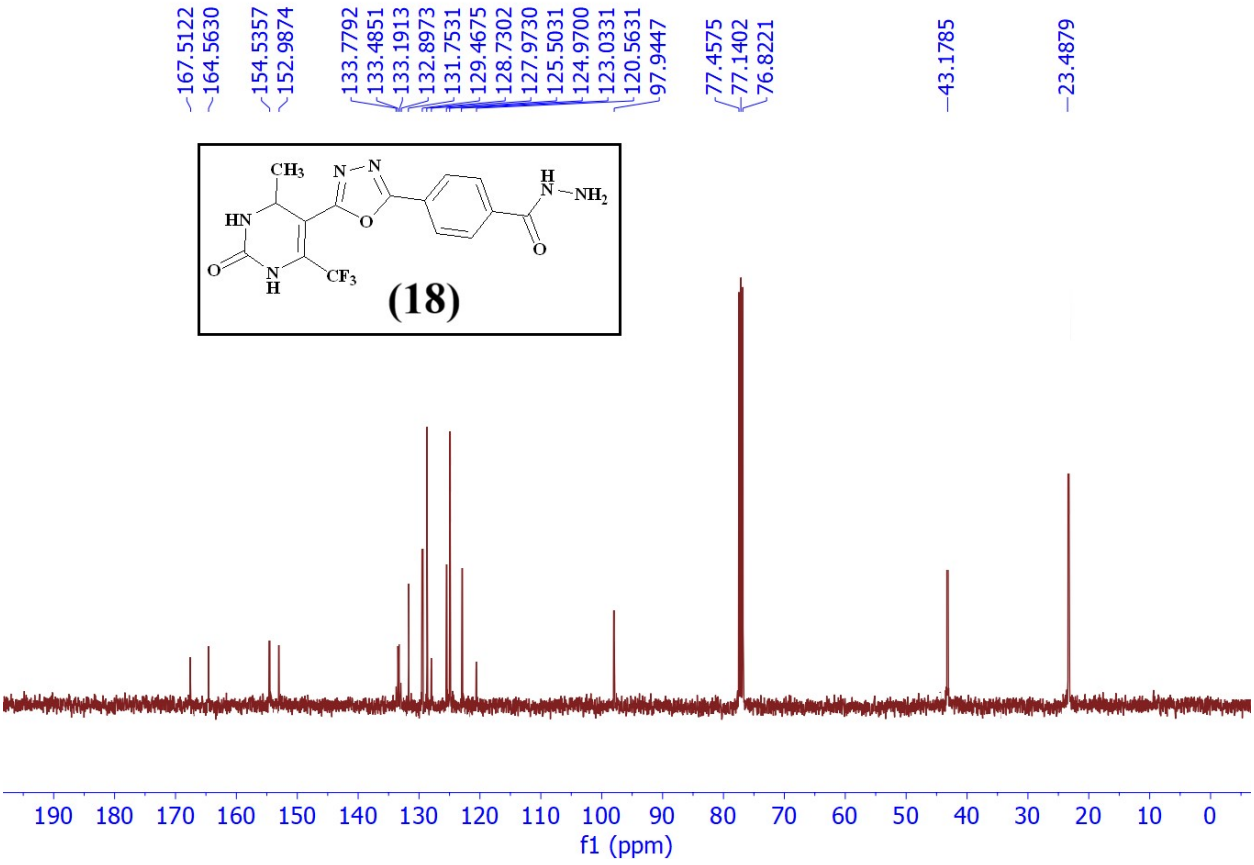

Figure S-11. ^{13}C NMR (100 MHz, $CDCl_3$) spectrum of compound **18.**

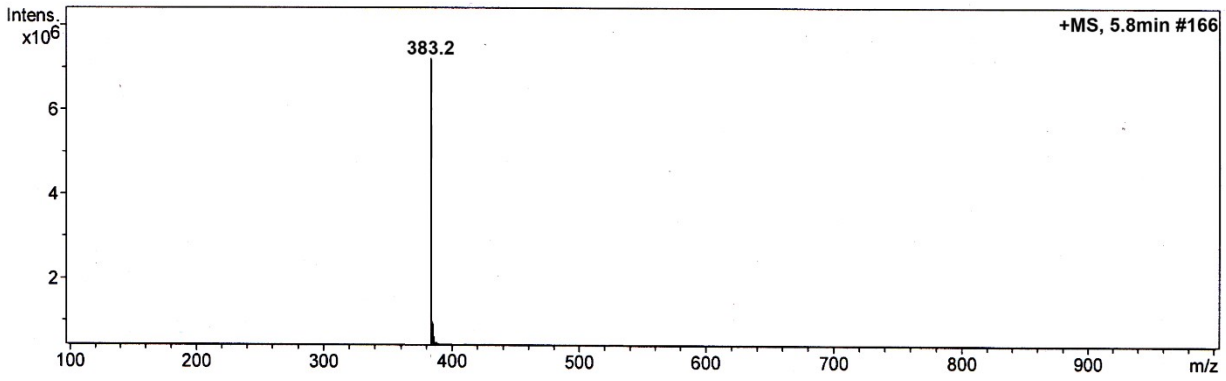

Figure S-12. LC-MS chromatogram of compound **18.**

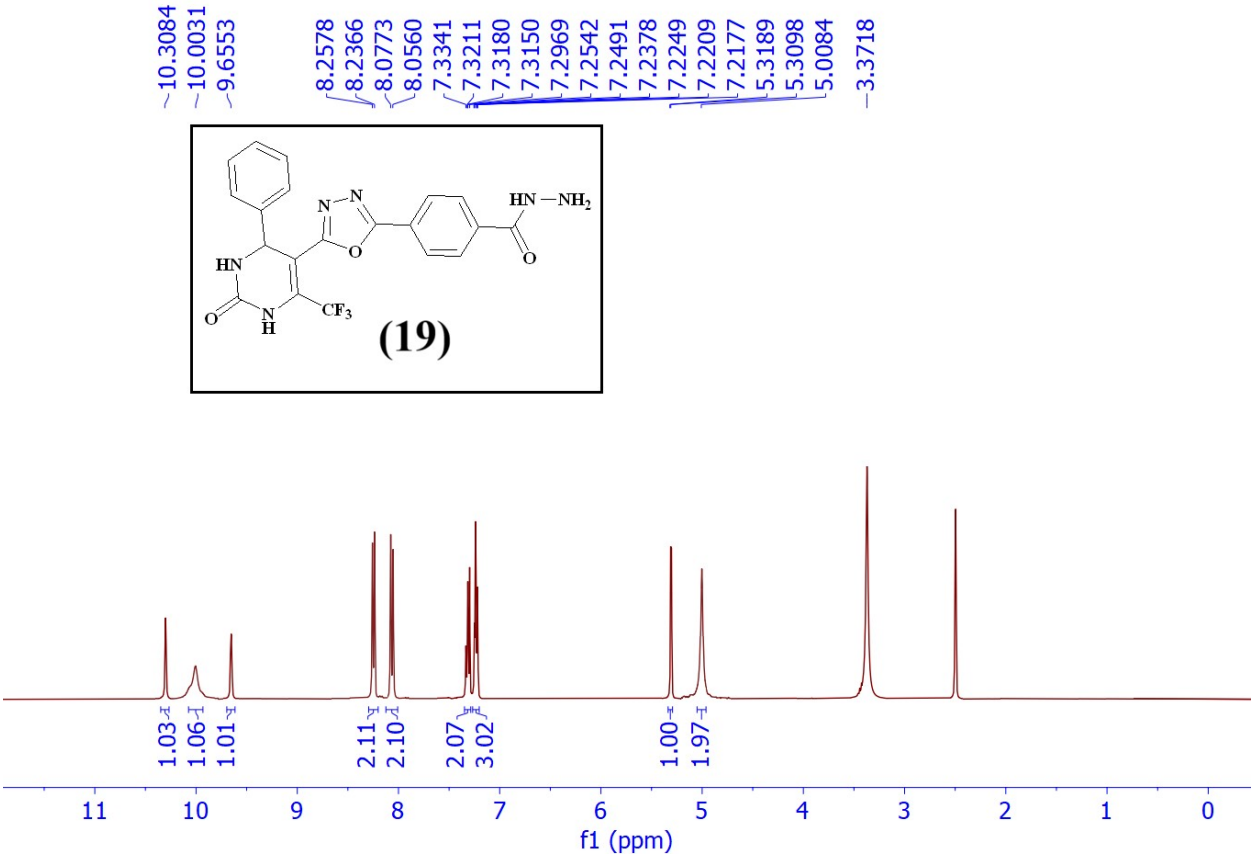

Figure S-13. ^{1}H NMR (400 MHz, DMSO-d_6) spectrum of compound **19.**

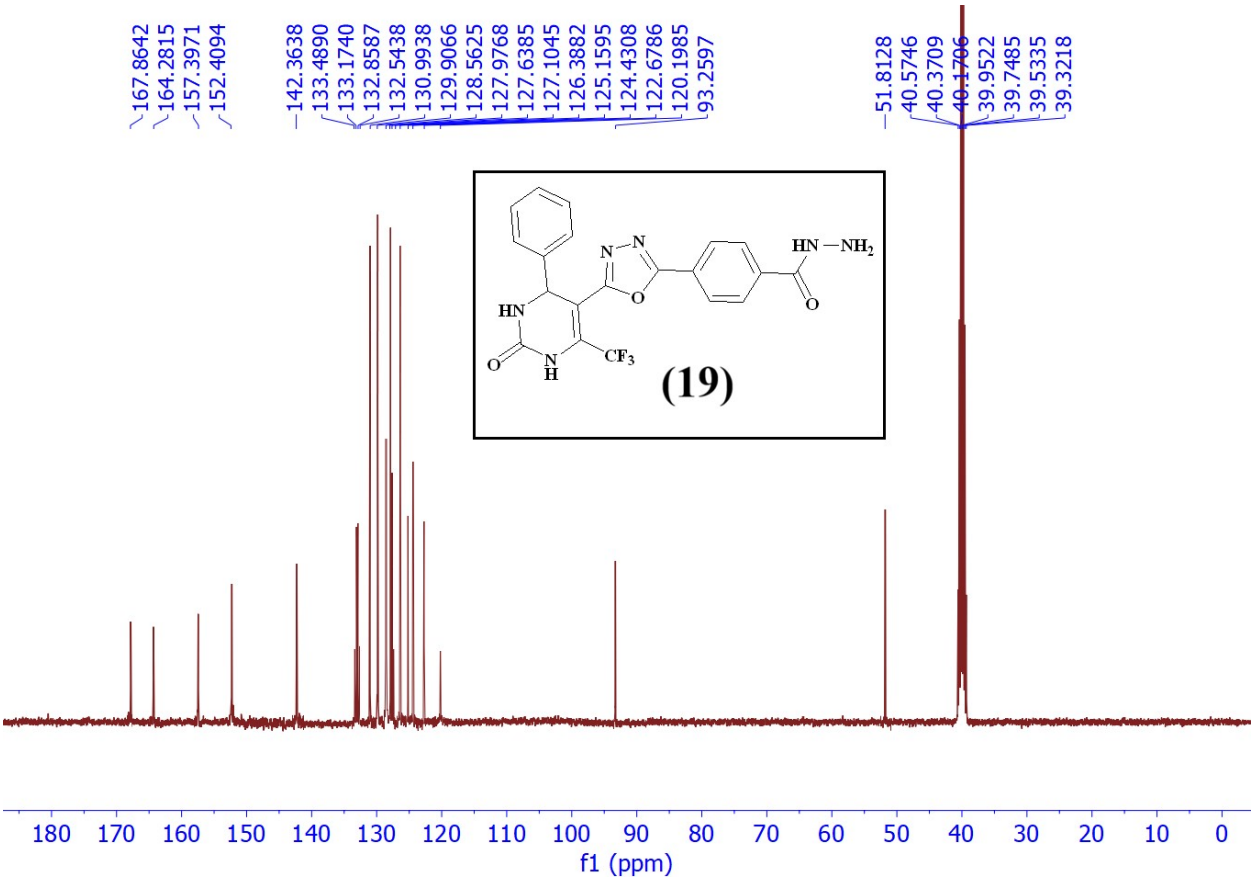

Figure S-14. ^{13}C NMR (100 MHz, DMSO-d_6) spectrum of compound **19.**

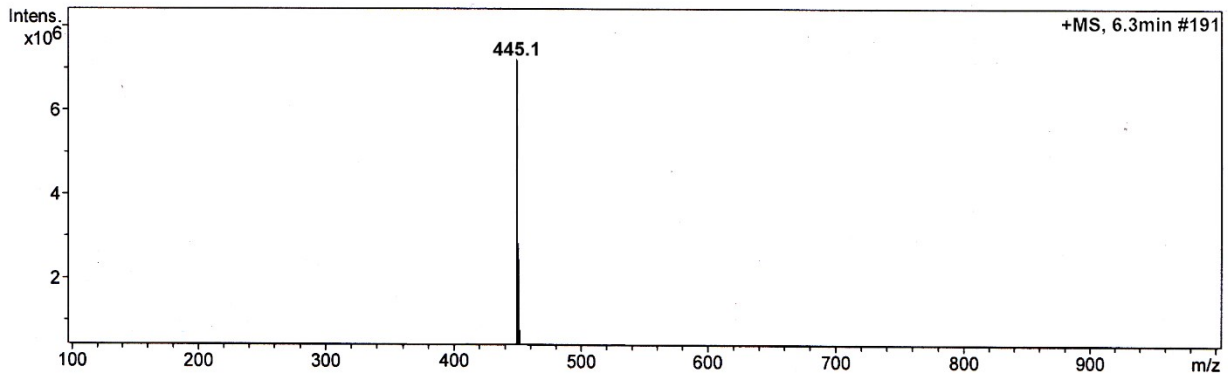

Figure S-15. LC-MS chromatogram of compound **19.**

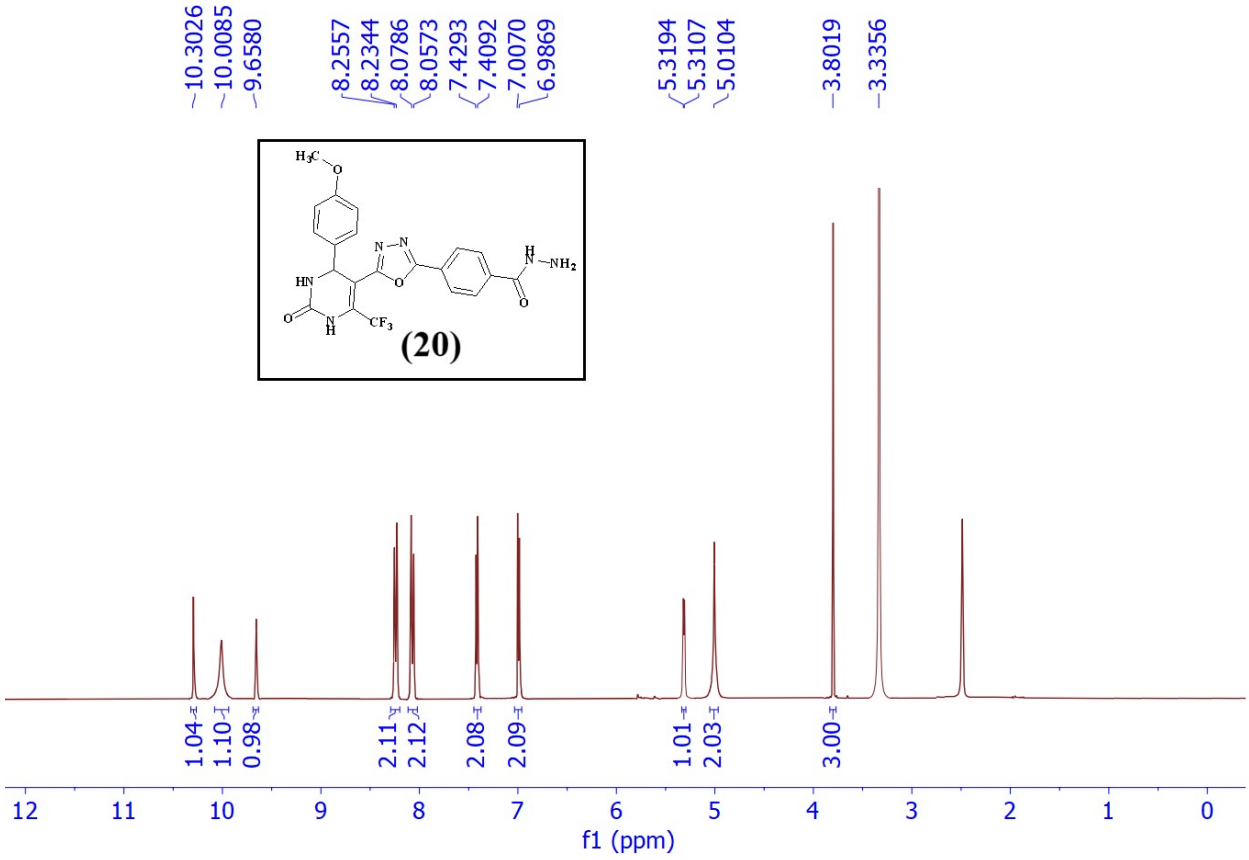

Figure S-16. ^{1}H NMR (400 MHz, DMSO-d_6) spectrum of compound **20.**

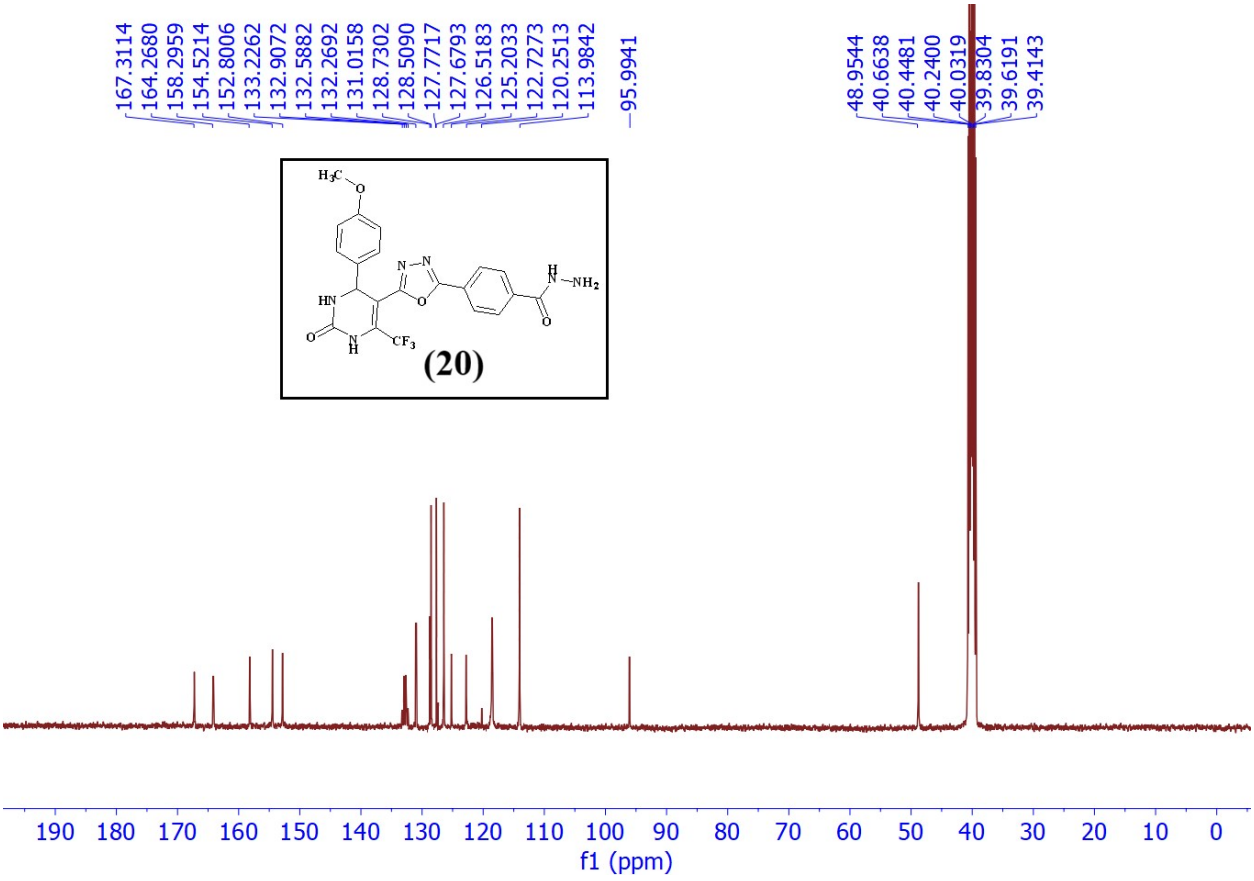

Figure S-17. ^{13}C NMR (100 MHz, DMSO-d_6) spectrum of compound **20.**

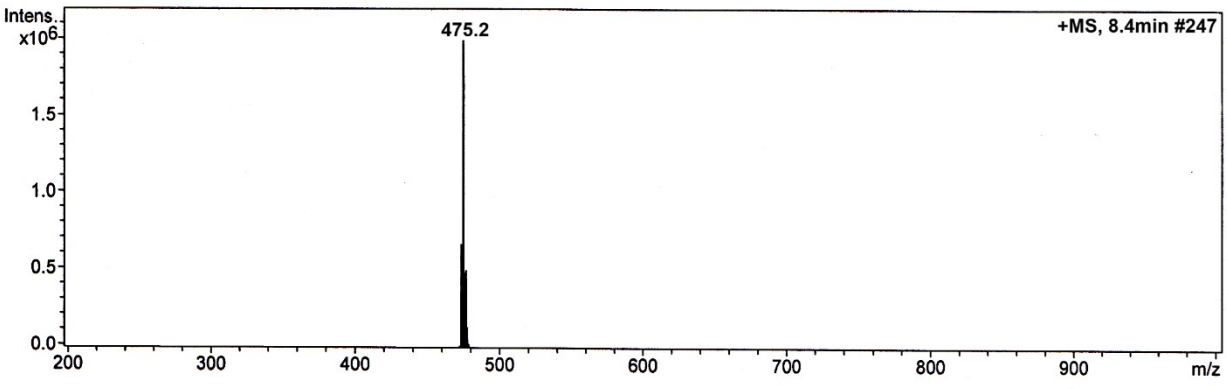

Figure S-18. LC-MS chromatogram of compound **20.**

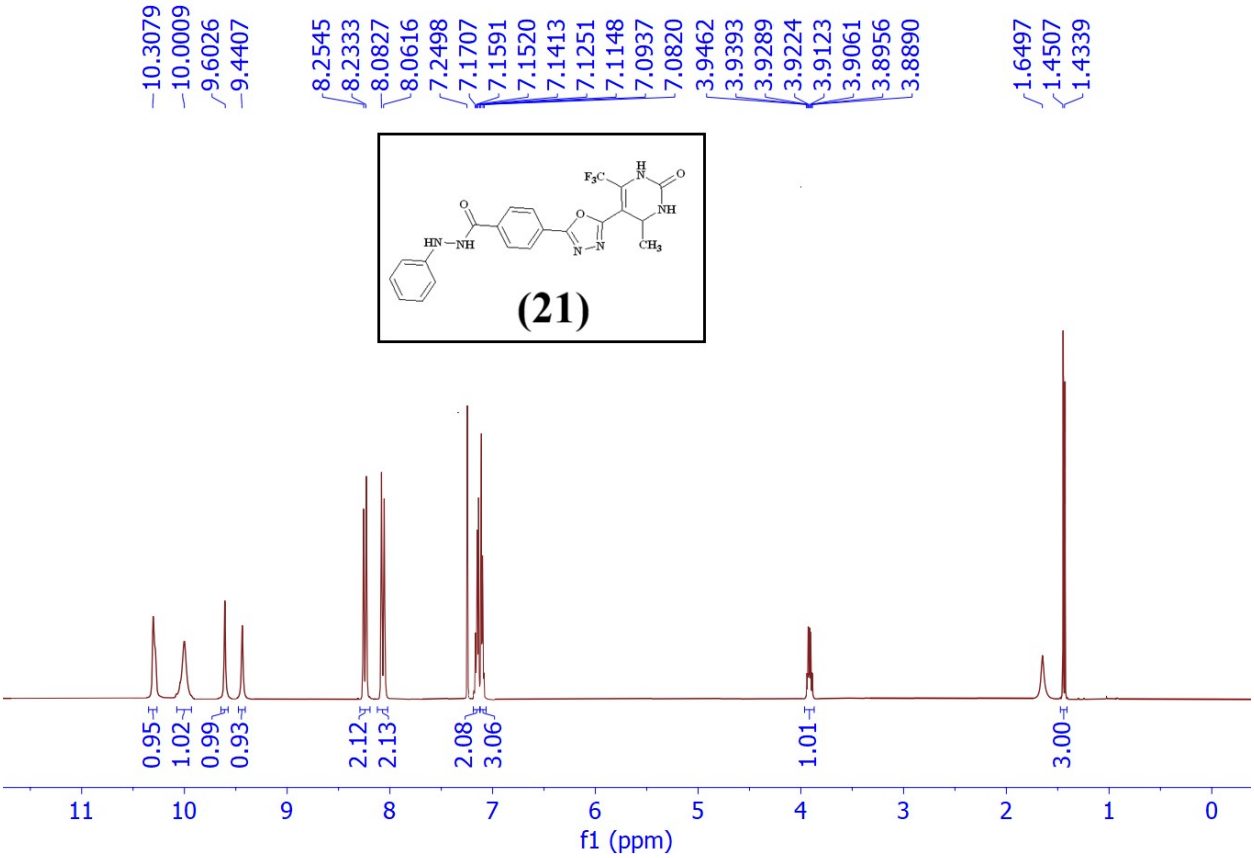

Figure S-19. ^{1}H NMR (400 MHz, $CDCl_3$) spectrum of compound **21.**

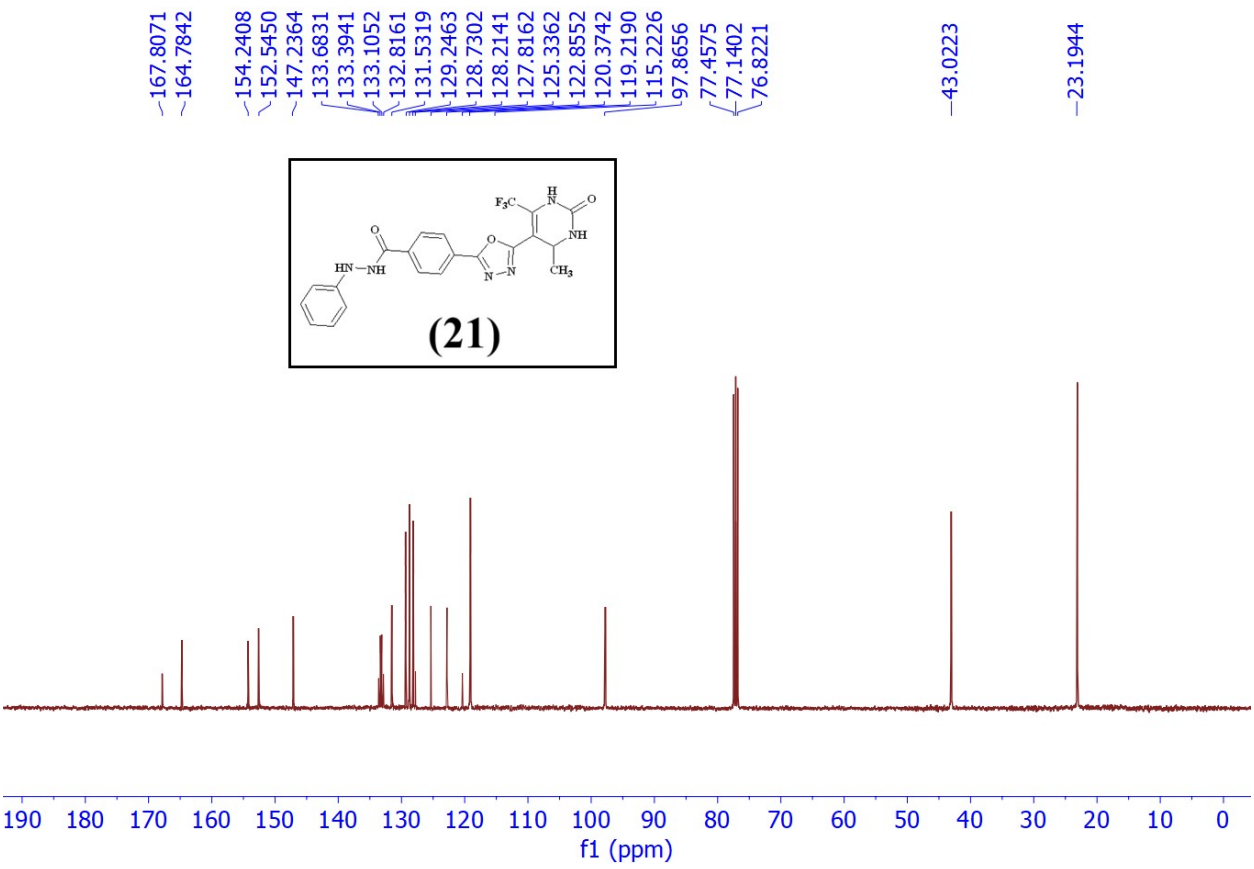

Figure S-20. ^{13}C NMR (100 MHz, $CDCl_3$) spectrum of compound **21.**

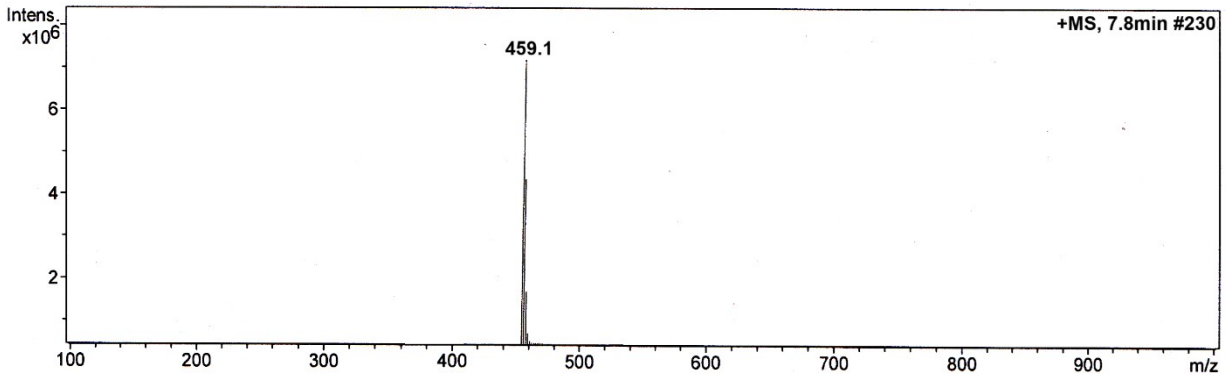

Figure S-21. LC-MS chromatogram of compound **21.**

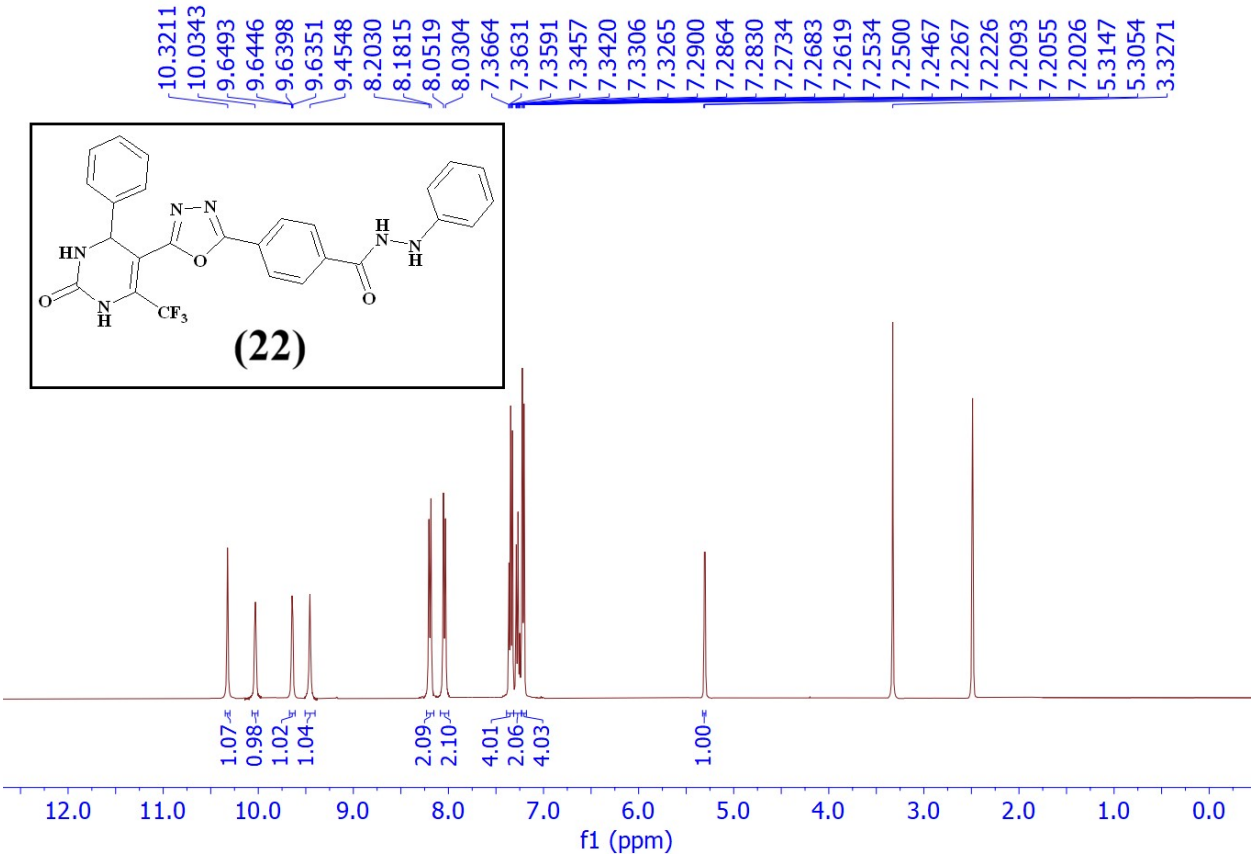

Figure S-22. ^{1}H NMR (400 MHz, DMSO-d_6) spectrum of compound **22.**

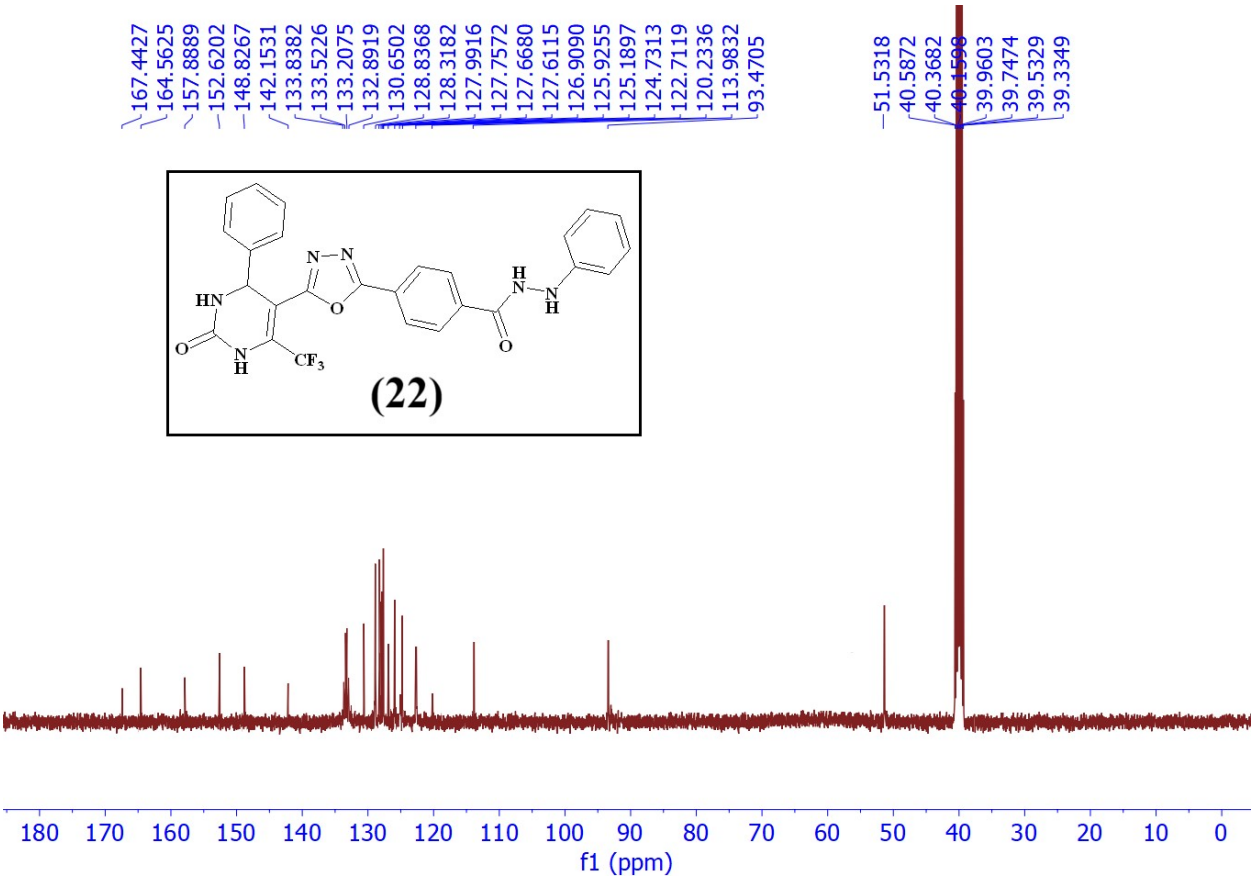

Figure S-23. ^{13}C NMR (100 MHz, DMSO-d_6) spectrum of compound **22.**

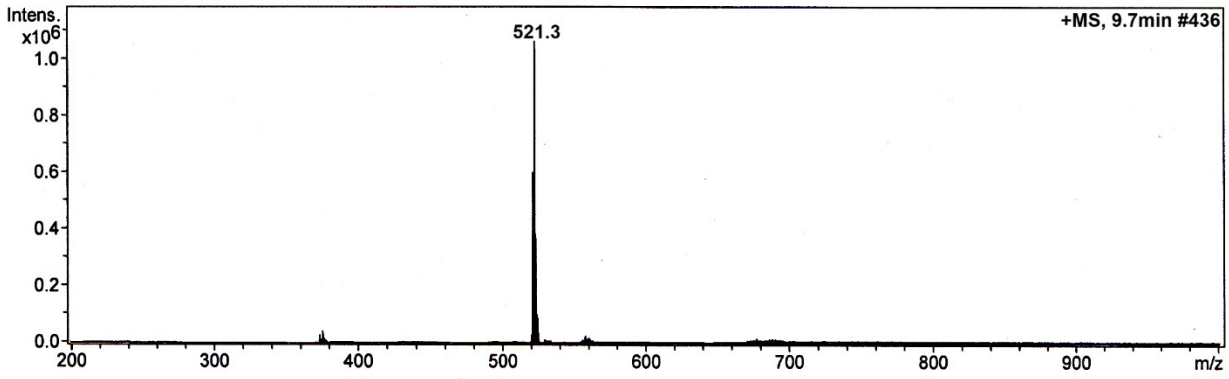

Figure S-24. LC-MS chromatogram of compound **22.**

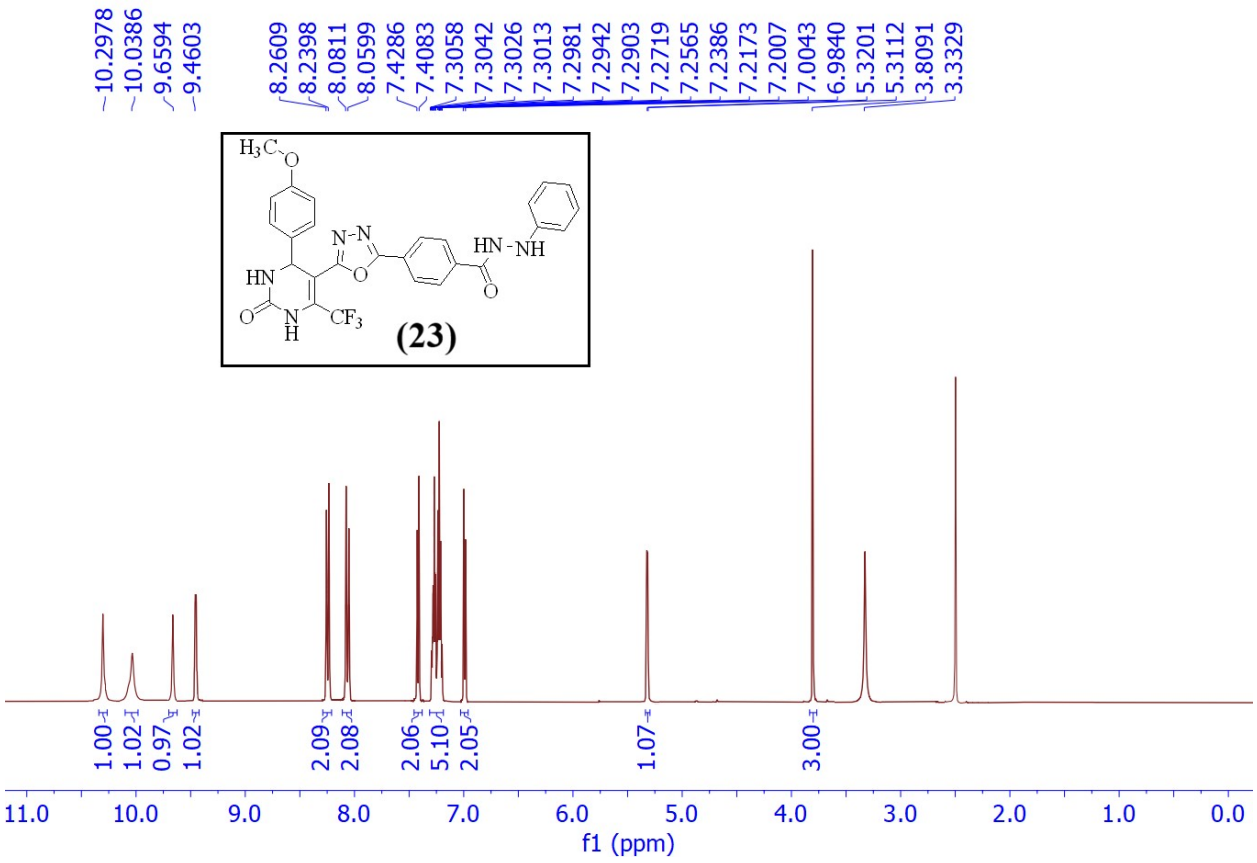

Figure S-25. ^{1}H NMR (400 MHz, DMSO-d_6) spectrum of compound **23.**

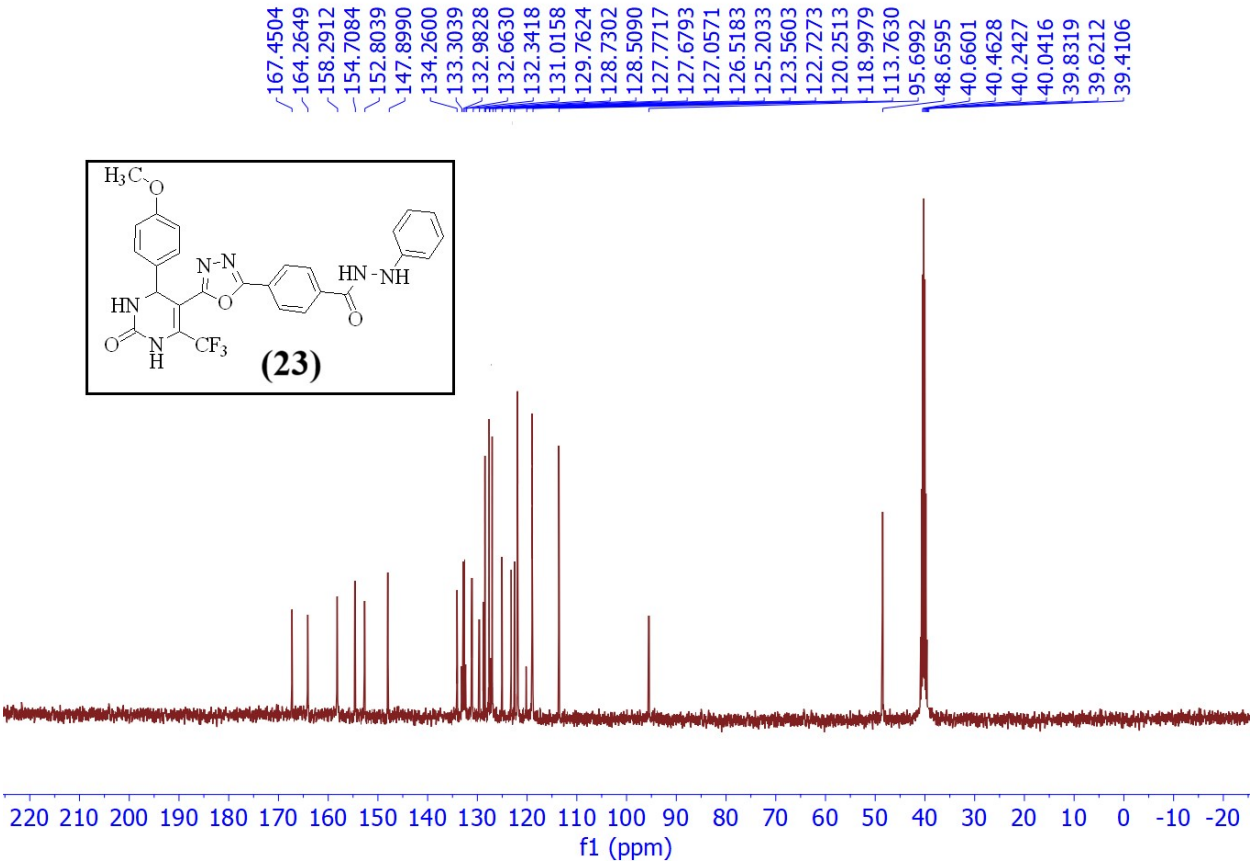

Figure S-26. ^{13}C NMR (100 MHz, DMSO-d_6) spectrum of compound **23.**

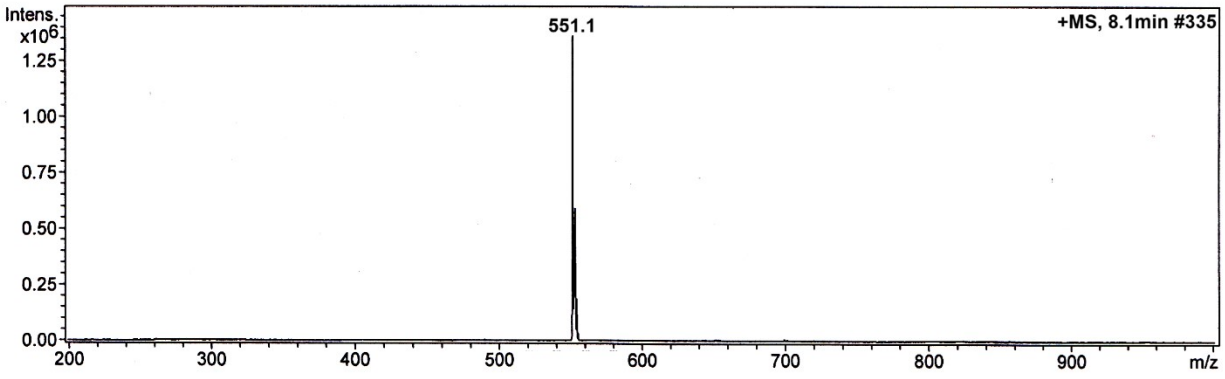

Figure S-27. LC-MS chromatogram of compound **23.**

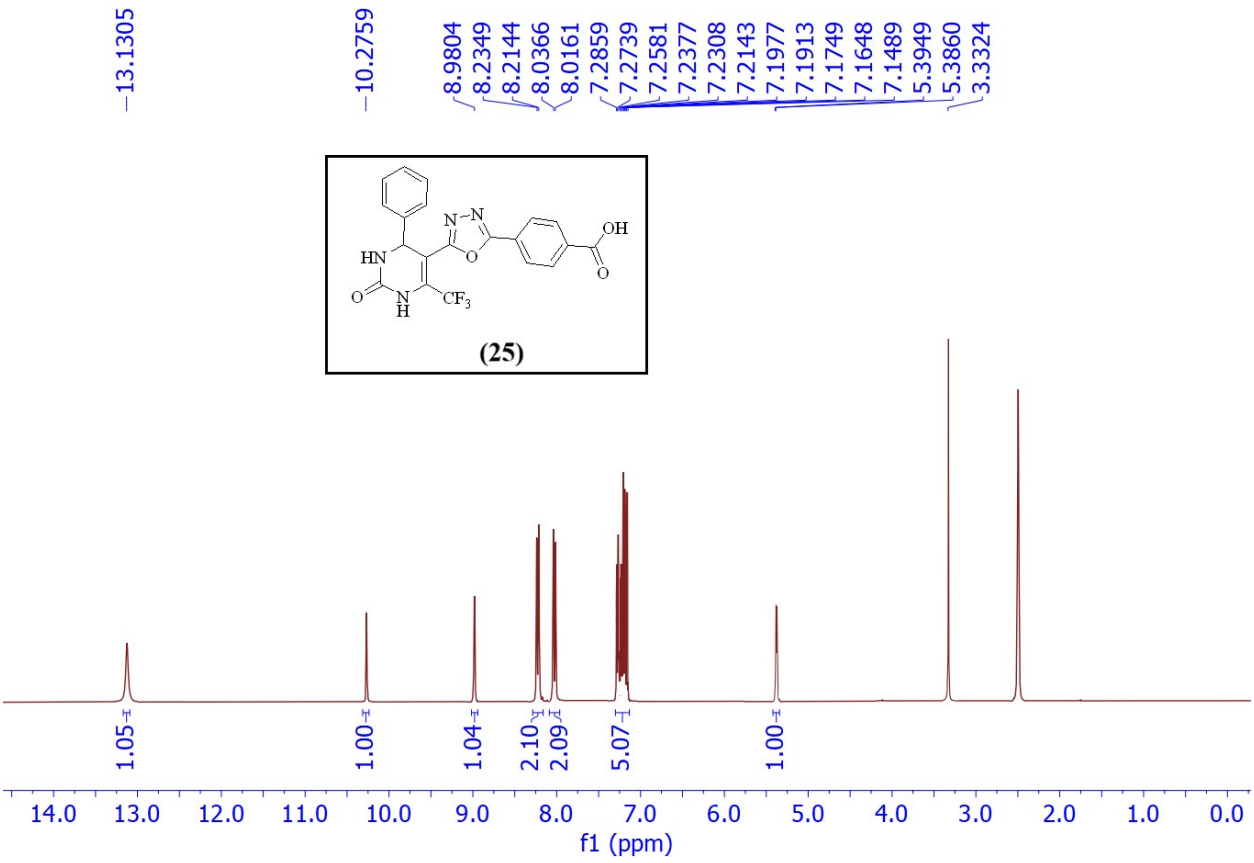

Figure S-28. ^{1}H NMR (400 MHz, DMSO-d_6) spectrum of Intermediate **25.**

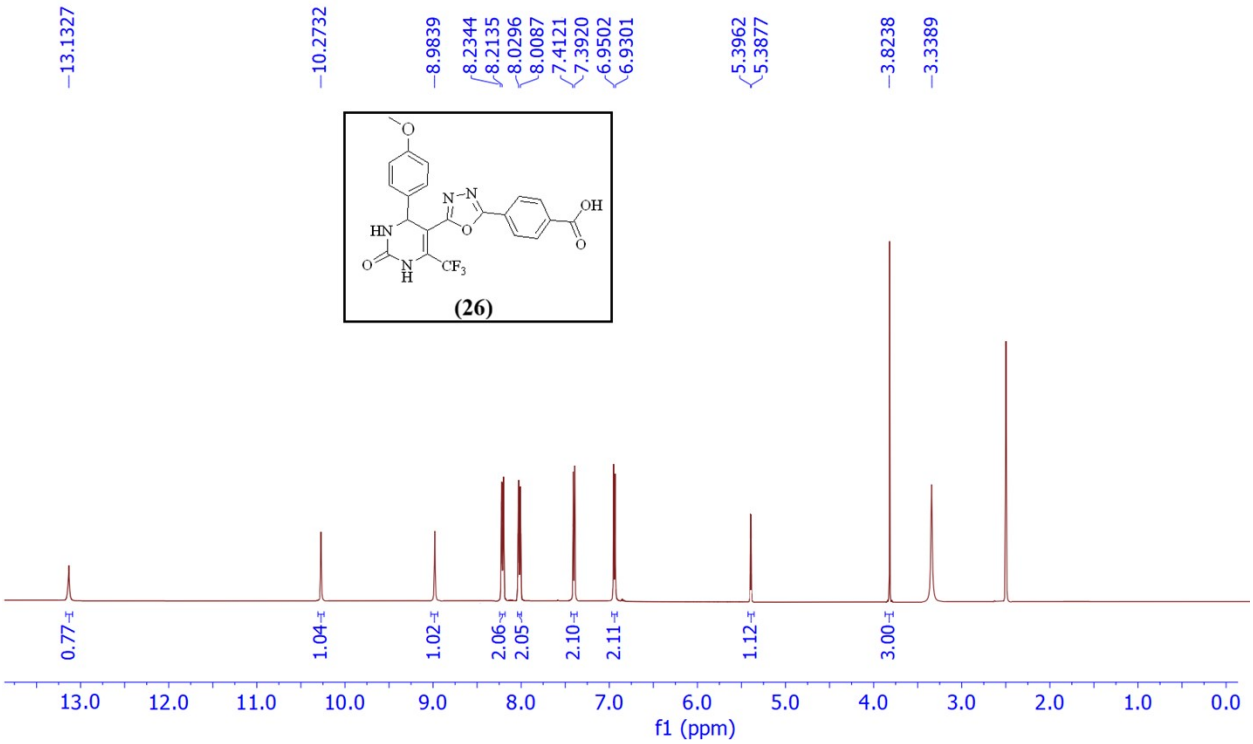

Figure S-29. ^{1}H NMR (400 MHz, DMSO-d_6) spectrum of Intermediate **26.**

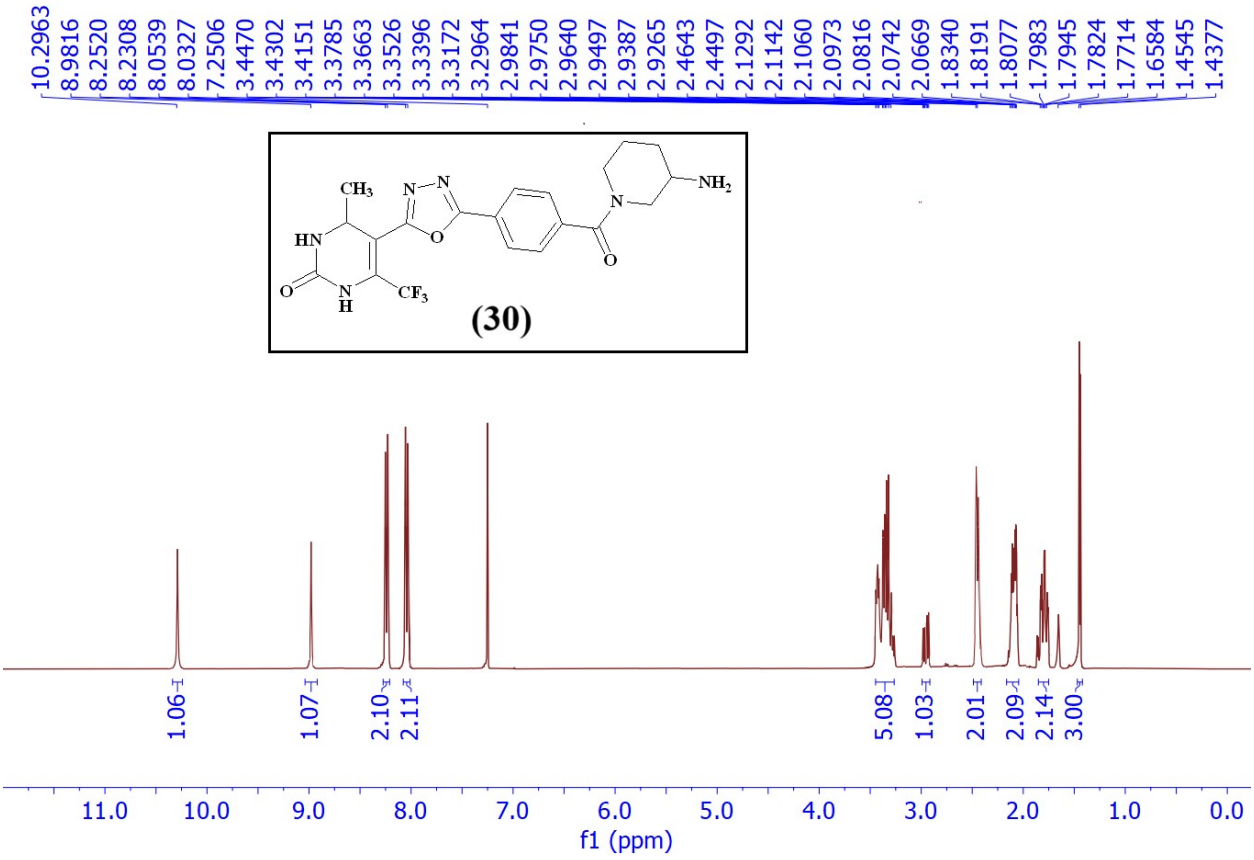

Figure S-30. ^{1}H NMR (400 MHz, $CDCl_3$) spectrum of Intermediate **30.**

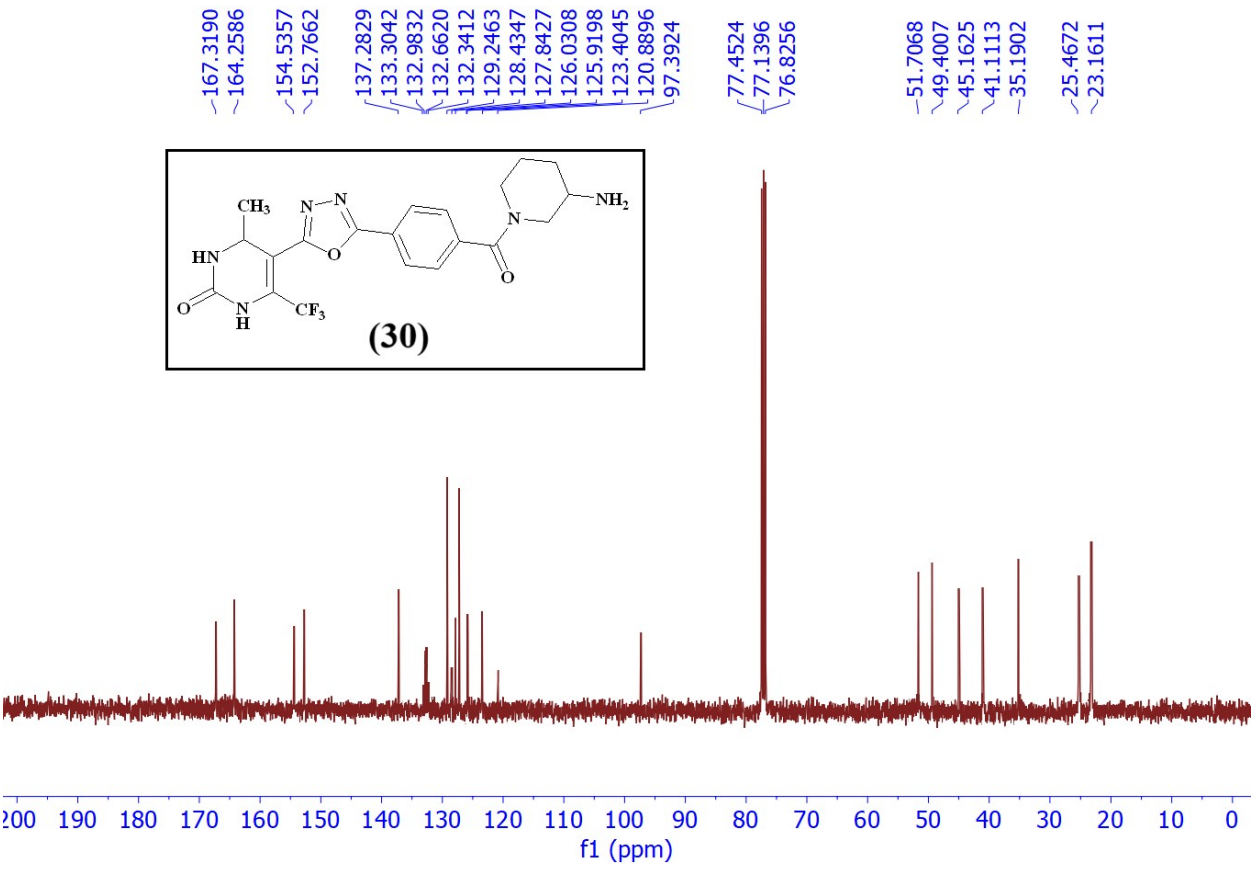

Figure S-31. ^{13}C NMR (100 MHz, DMSO-d_6) spectrum of compound **30.**

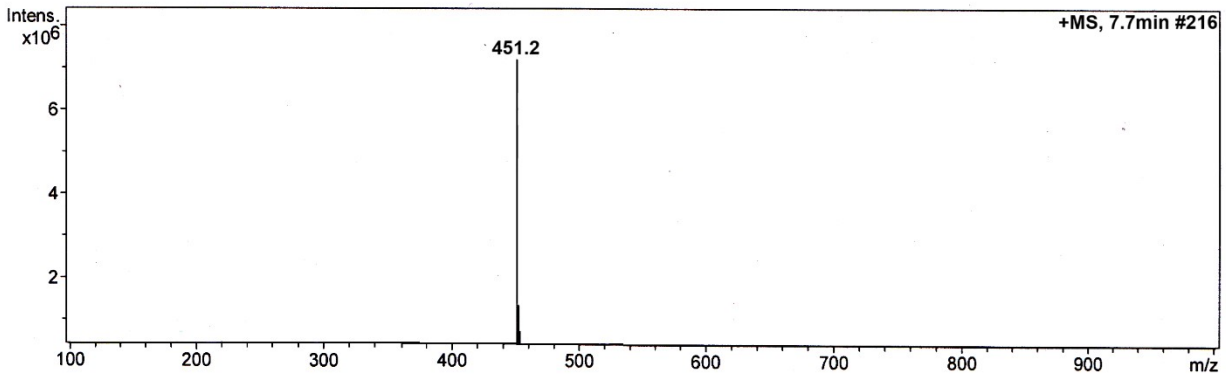

Figure S-32. LC-MS chromatogram of compound **30.**

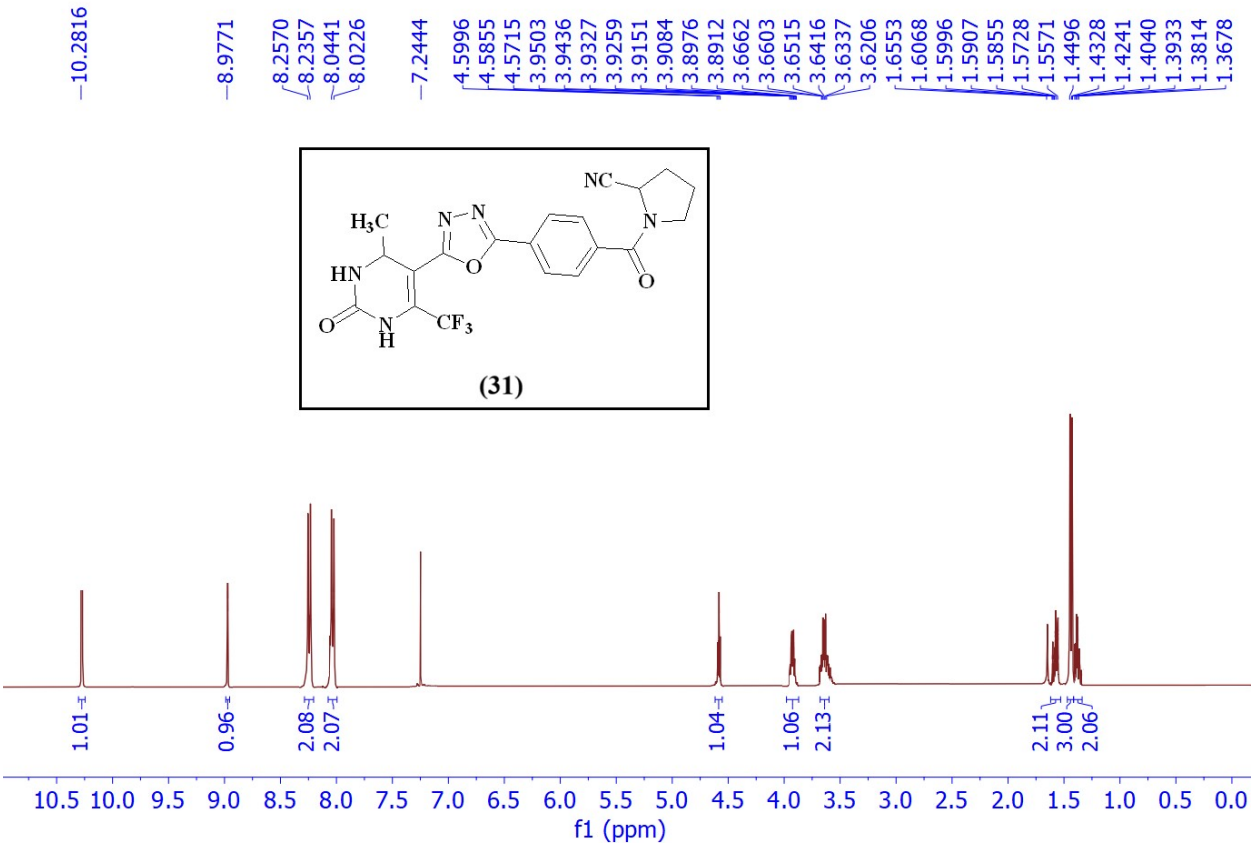

Figure S-33. ^{1}H NMR (400 MHz, $CDCl_3$) spectrum of Intermediate **31.**

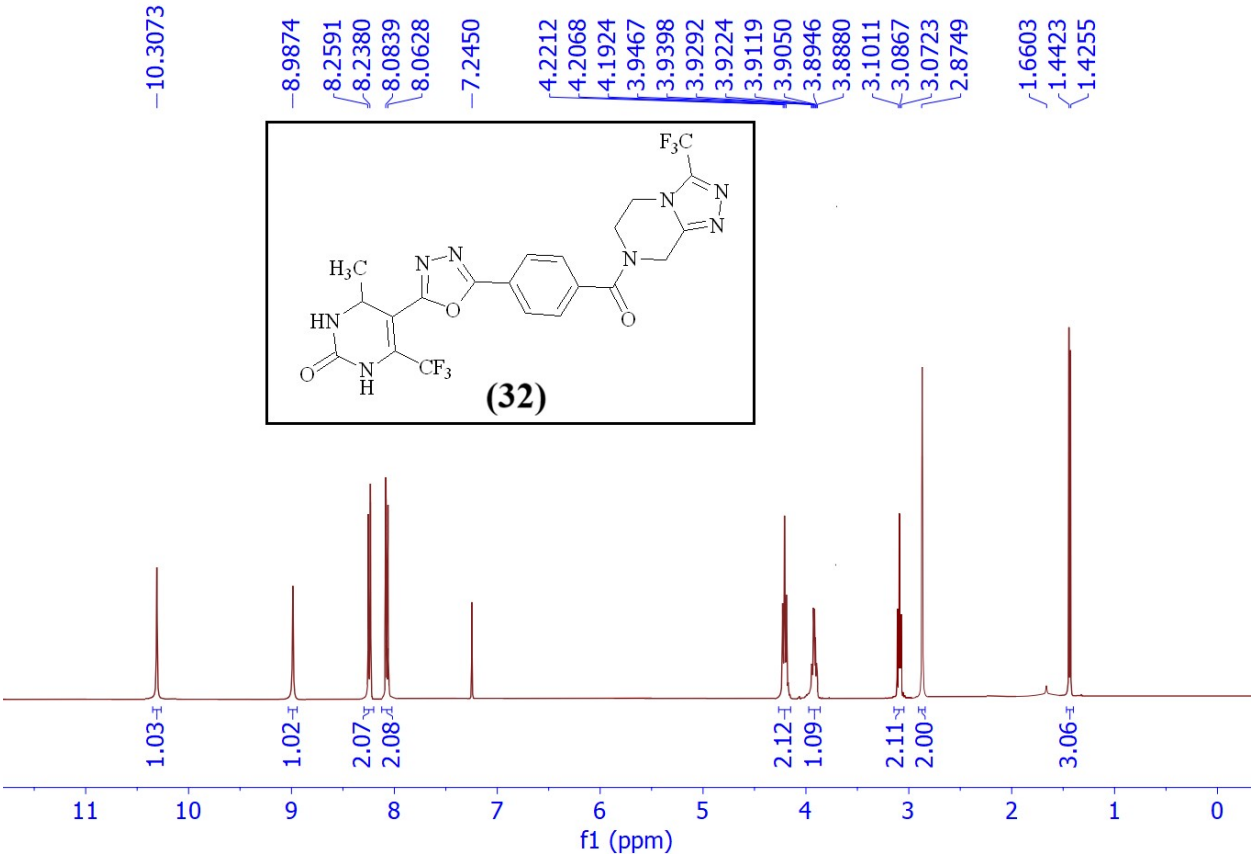

Figure S-34. ^{1}H NMR (400 MHz, $CDCl_3$) spectrum of compound **32.**

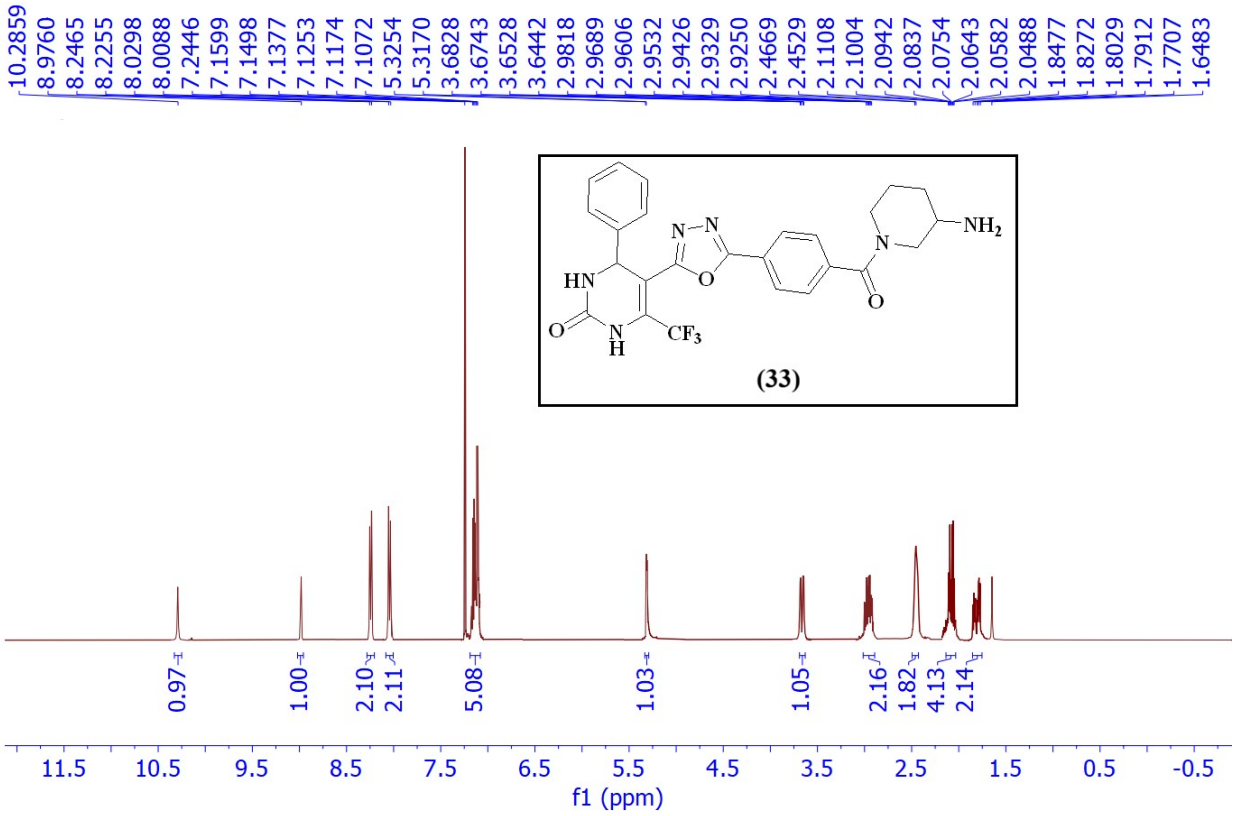

Figure S-35. ^{1}H NMR (400 MHz, $CDCl_3$) spectrum of compound **33.**

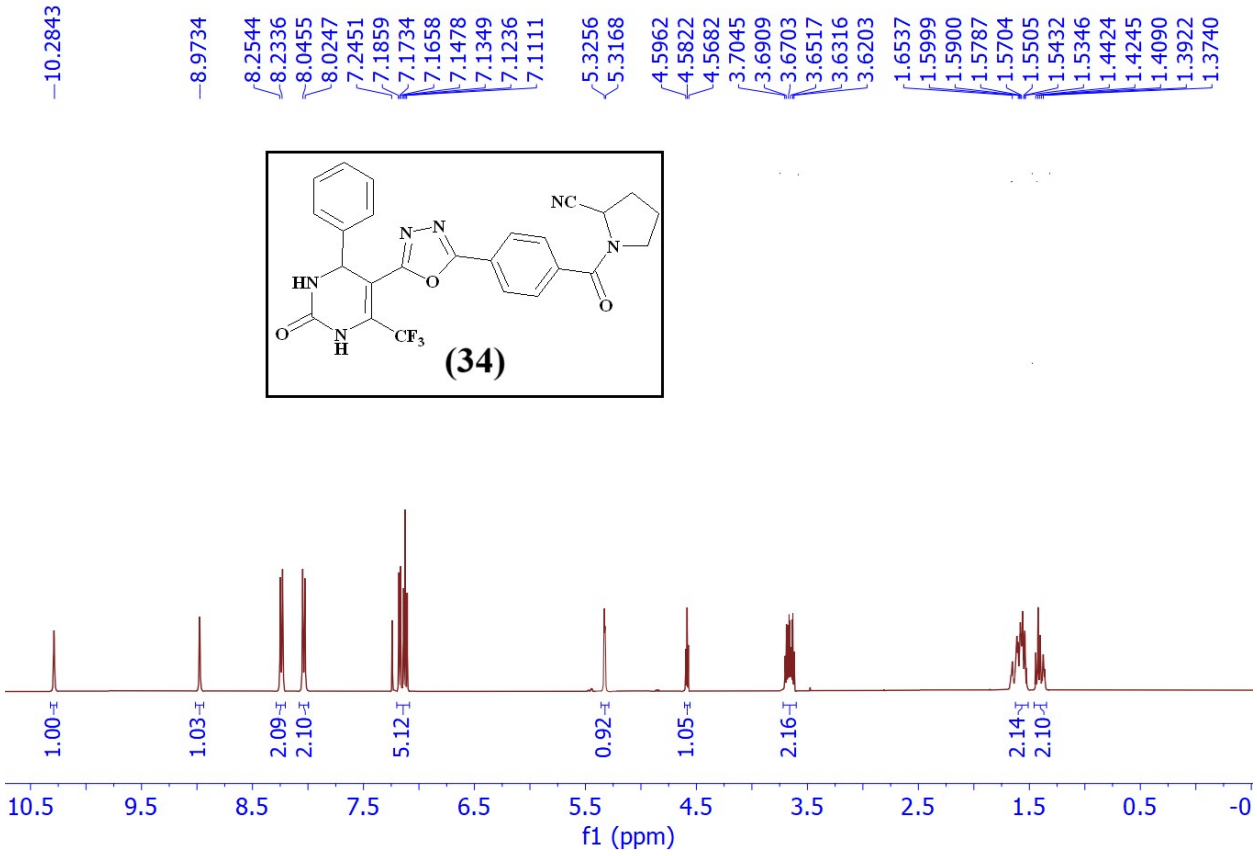

Figure S-36. ^{1}H NMR (400 MHz, $CDCl_3$) spectrum of compound **34.**

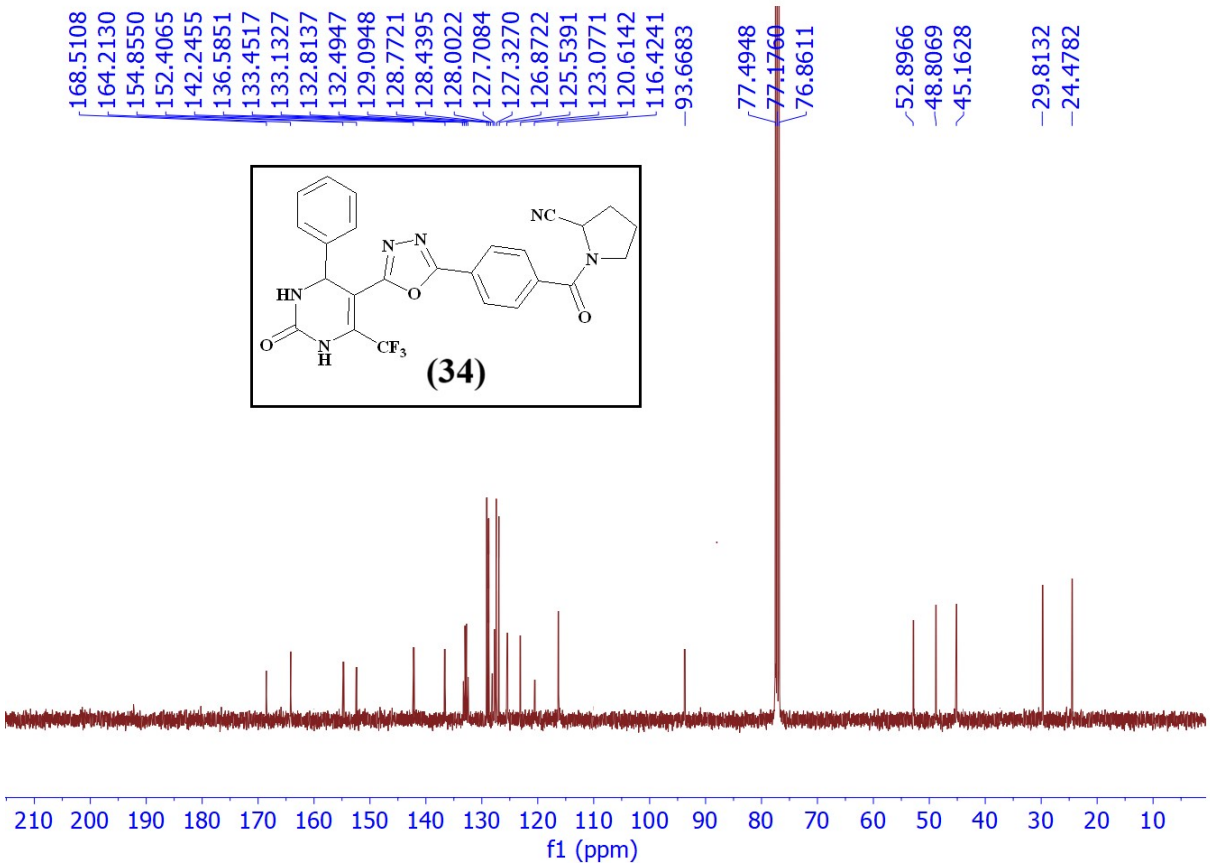

Figure S-37. ^{13}C NMR (100 MHz, $CDCl_3$) spectrum of compound **34.**

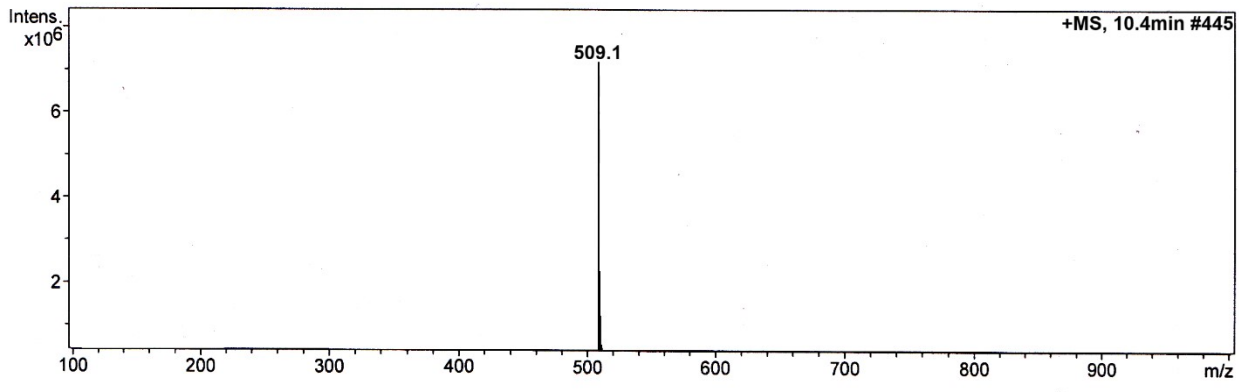

Figure S-38. LC-MS chromatogram of compound **34.**

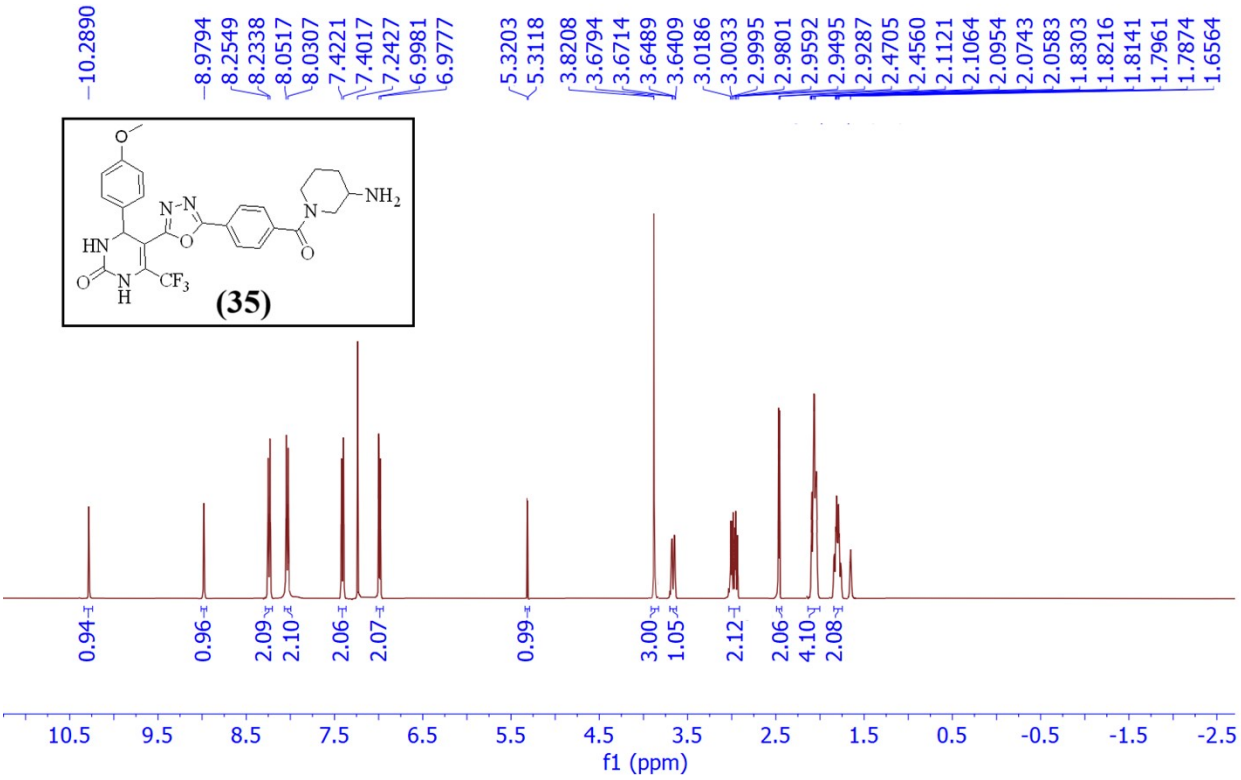

Figure S-39. ^{1}H NMR (400 MHz, $CDCl_3$) spectrum of compound **35.**

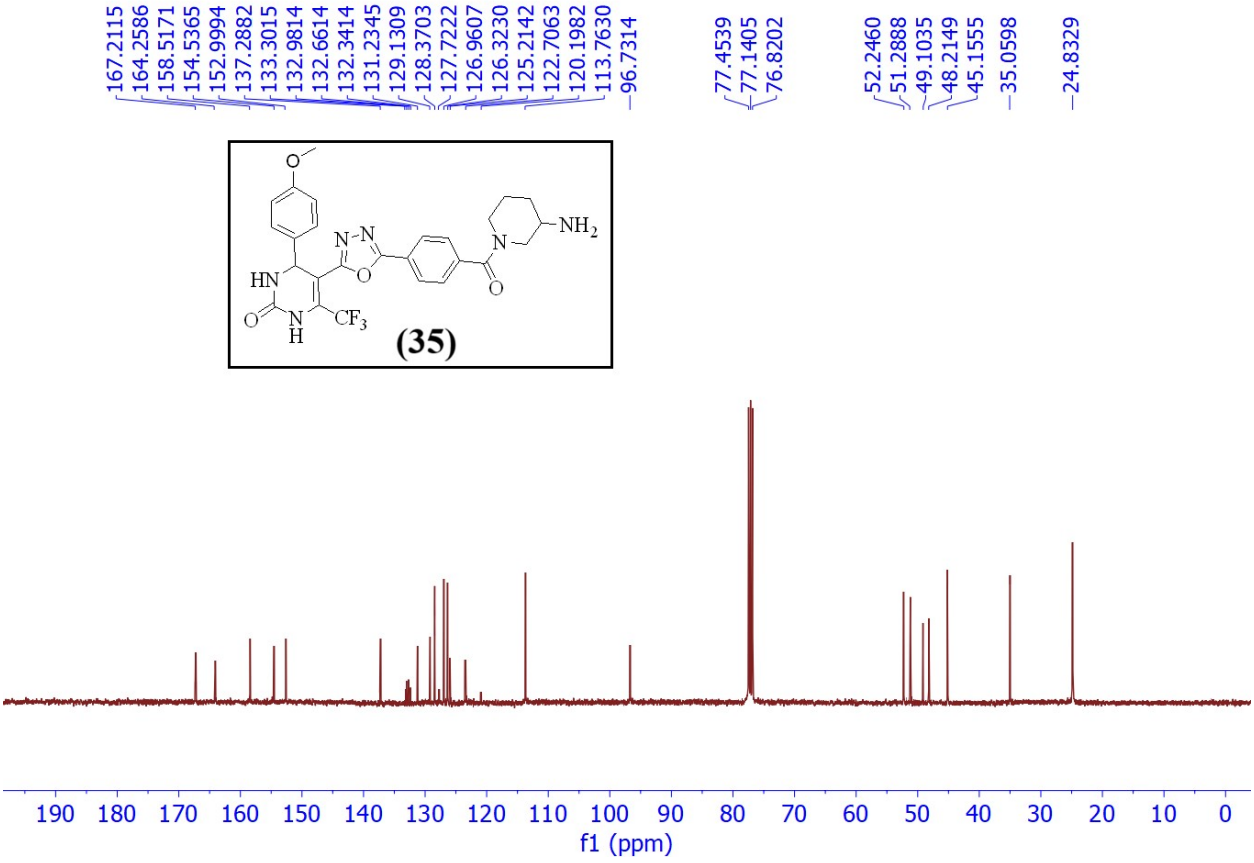

Figure S-40. ^{13}C NMR (100 MHz, $CDCl_3$) spectrum of compound **35.**

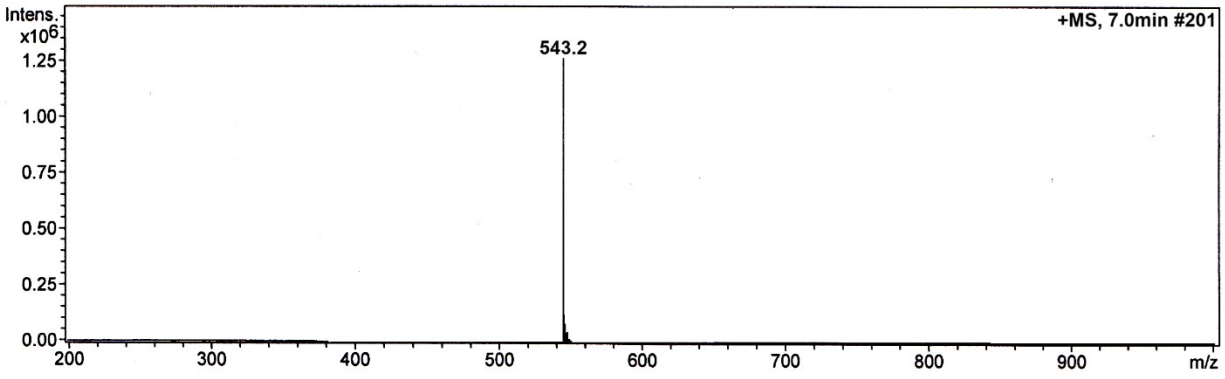

Figure S-41. LC-MS chromatogram of compound **35.**

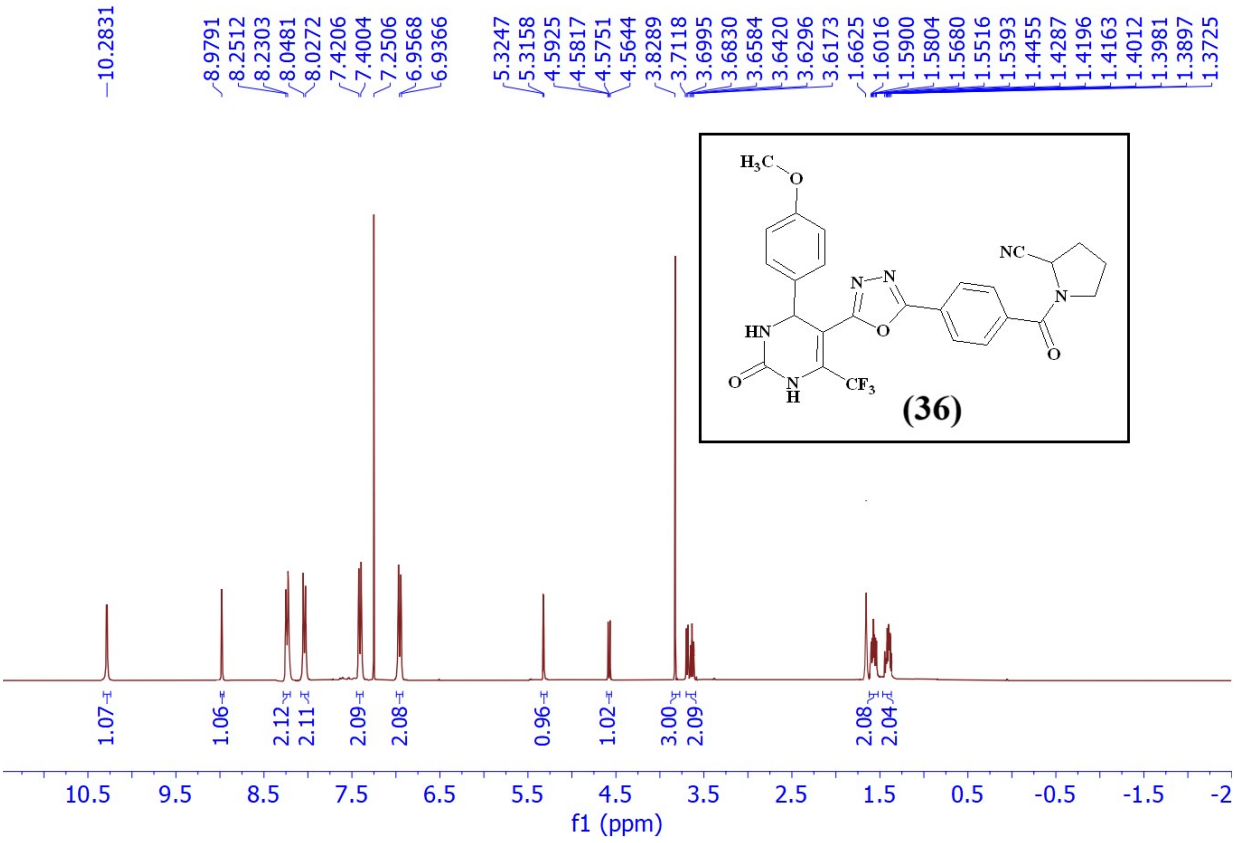

Figure S-42. ^{1}H NMR (100 MHz, $CDCl_3$) spectrum of compound **36.**

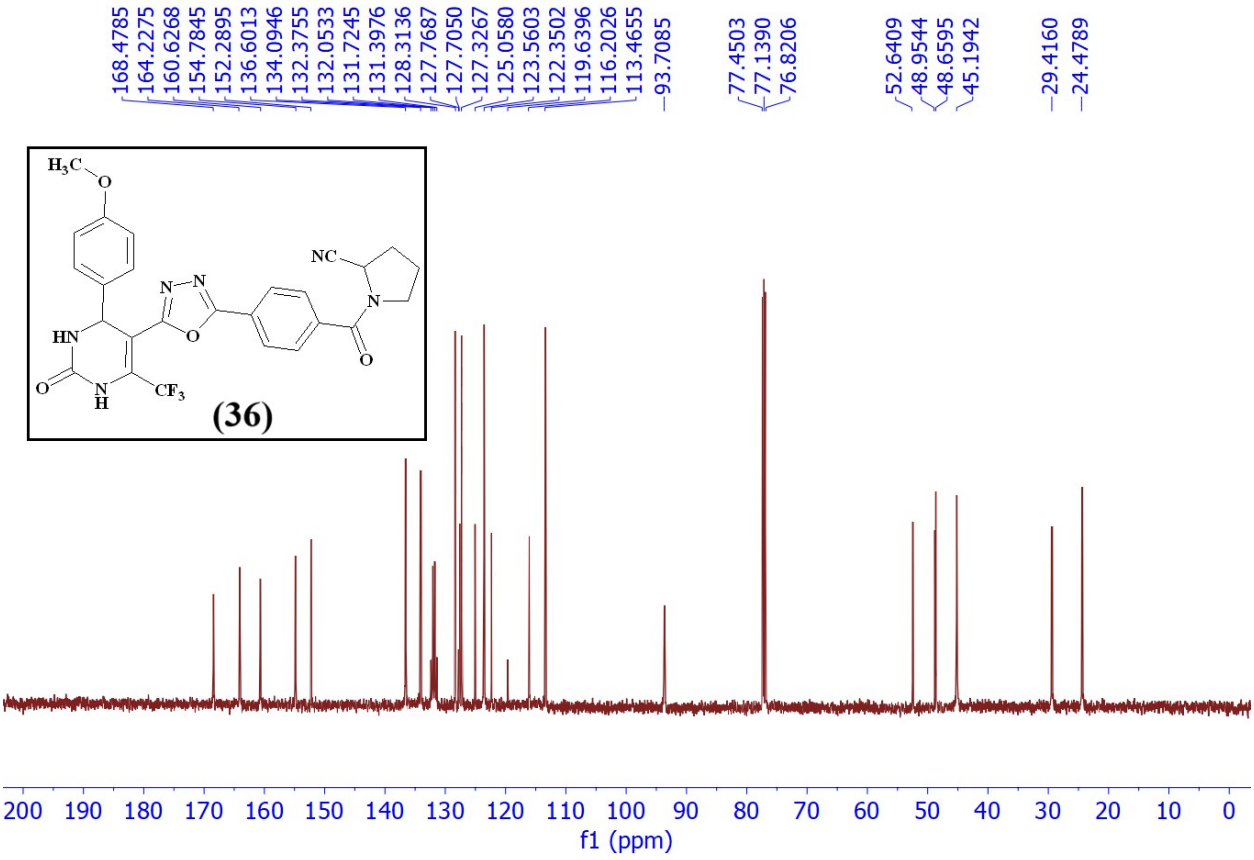

Figure S-43. ^{13}C NMR (100 MHz, $CDCl_3$) spectrum of compound **36.**

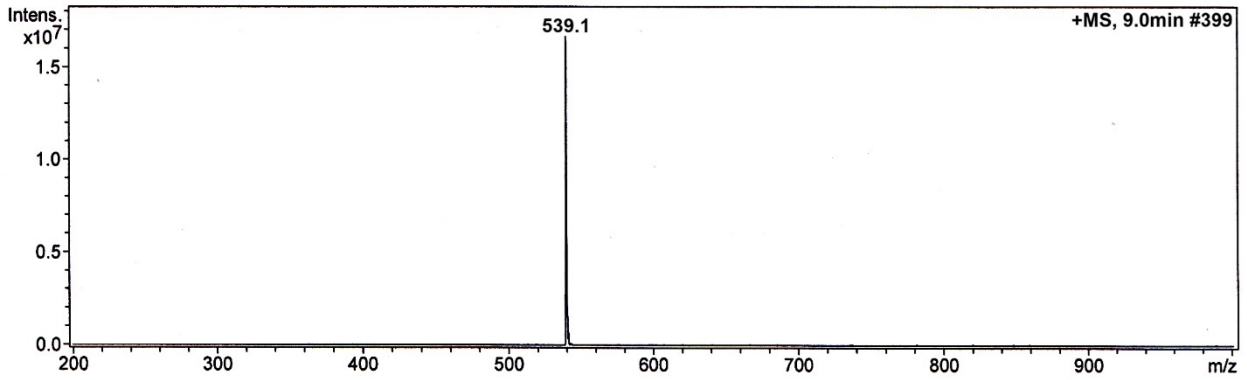

Figure S-44. LC-MS chromatogram of compound **36.**